BAND MODEL CALCULATION OF ATMOSPHERIC TRANSMITTANCE FOR HOT GAS LINE EMISSION SOURCES. ACCOUNT OF DOPPLER BROADENING

Stephen J. Young

Aerospace Corporation

Prepared for:

Space and Missile Systems Organization
Defense Advanced Research Projects Agency

30 July 1975

REPORT SAMSO-TR-75-212

Band Model Calculation of Atmospheric Transmittance for Hot Gas Line Emission Sources

Account of Doppler Broadening

S. J. YOUNG
Chemistry and Physics Laboratory
Laboratory Operations
The Aerospace Corporation
El Segundo, Calif. 90245

30 July 1975

Interim Report

Sponsored by
DEFENSE ADVANCED RESEARCH PROJECTS AGENCY
1400 Wilson Blvd
Arlington, Va. 22209

DARPA Order No. 2843

SPACE AND MISSILE SYSTEMS ORGANIZATION
AIR FORCE SYSTEMS COMMAND
Los Angeles Air Force Station
Los Angeles, Calif. 90045

This research was supported by the Defense Advanced Research Projects Agency of the Department of Defense and was monitored by Space and Missile Systems Organization (SAMSO) under Contract No. F04701-74-C-0075.

Approved

S. Siegel, Director
Chemistry and Physics Laboratory

This technical report has been reviewed and is approved. Approval of this report does not constitute Air Force approval of the report's findings or conclusions. It is published only for the exchange and stimulation of ideas.

FOR THE COMMANDER

Jimmy D. Lamb
Col., United States Air Force
Director, Development Directorate
Deputy for Technology

UNCLASSIFIED

SECURITY CLASSIFICATION OF THIS PAGE (When Data Entered)

REPORT DOCUMENTATION PAGE		READ INSTRUCTIONS BEFORE COMPLETING FORM
1. REPORT NUMBER SAMSO-TR-75-212	2. GOVT ACCESSION NO.	3. RECIPIENT'S CATALOG NUMBER
4. TITLE (and Subtitle) BAND MODEL CALCULATIONS OF ATMOSPHERIC TRANSMITTANCE FOR HOT GAS LINE EMISSION SOURCES. Account of Doppler Broadening		5. TYPE OF REPORT & PERIOD COVERED Interim 6. PERFORMING ORG. REPORT NUMBER TR-0076(6970)-5
7. AUTHOR(s) Stephen J. Young		8. CONTRACT OR GRANT NUMBER(s) F04701-75-C-0076
9. PERFORMING ORGANIZATION NAME AND ADDRESS The Aerospace Corporation El Segundo, Calif. 90245		10. PROGRAM ELEMENT, PROJECT, TASK AREA & WORK UNIT NUMBERS
11. CONTROLLING OFFICE NAME AND ADDRESS Defense Advanced Research Projects Agency 1400 Wilson Blvd. Arlington, Va. 22209		12. REPORT DATE 30 July 1975 13. NUMBER OF PAGES 62
14. MONITORING AGENCY NAME & ADDRESS (if different from Controlling Office) Space and Missile Systems Organization Air Force Systems Command Los Angeles, Calif. 90045		15. SECURITY CLASS. (of this report) Unclassified 15a. DECLASSIFICATION/DOWNGRADING SCHEDULE

16. DISTRIBUTION STATEMENT (of this Report)

Approved for public release; distribution unlimited.

17. DISTRIBUTION STATEMENT (of the abstract entered in Block 20, if different from Report)

18. SUPPLEMENTARY NOTES

19. KEY WORDS (Continue on reverse side if necessary and identify by block number)

Band Model Formulation
Inhomogeneous Optical Paths
Atmospheric Transmittance
Doppler Broadening Correction
Voigt Line Shape
Hot Gas Emission

20. ABSTRACT (Continue on reverse side if necessary and identify by block number)

Results of band model calculations for the effective transmittance of the atmosphere to radiation from hot gaseous H_2O/CO_2 emission sources are reported. The source model represents a missile plume in the sea level to z = 60 km altitude range. The effective transmittances along a slant path from the source altitude to space at a zenith angle of 75 deg are computed and averaged over three wide bandpasses in the 2.7-μm spectral region. Statistical band model calculations are performed for the assumption that the emission-absorption lines have a Lorentz, Doppler, or Voigt

DD FORM 1473 (FACSIMILE)

UNCLASSIFIED

SECURITY CLASSIFICATION OF THIS PAGE (When Data Entered)

19 KEY WORDS (Continued)

20 ABSTRACT (Continued)

profile. The approximation used to handle the Voigt profile is discussed. Inhomogeneities inherent in treating the line of sight through the atmosphere and the hot gas source as a single, highly inhomogeneous optical path are accounted for by using either the Curtis-Godson, the Lindquist-Simmons, or the two-path derivative approximation. The latter is derived herein and is shown to be superior to the Lindquist-Simmons approximation in treating radiative transfer calculations for the Doppler or Voigt line shape.

The results indicate that, for source altitudes above about 25 km, the line shape cannot be assumed to be a pressure-broadened Lorentz line; Doppler broadening effects must be included by using the Voigt profile. With line shape properly accounted for, the results still indicate a large difference between the effective atmospheric transmittance $\bar{\tau}_e$ and the atmospheric transmittance $\bar{\tau}$ appropriate for continuum emission. This large difference can result only from the high degree of line correlation that exists between the hot H_2O/CO_2 emission spectrum and the cool H_2O/CO_2 atmospheric absorption spectrum. Even at z = 60 km for the 3575-3725 cm^{-1} bandpass, the average value of $\bar{\tau}_e$ is only 0.8, whereas the average value of $\bar{\tau}$ is 0.99.

CONTENTS

FIGURES

TABLES

I. INTRODUCTION

In a previous report,[1] band model methods were used to compute the effective transmittance of the atmosphere for radiation emitted by a high-temperature gaseous H_2O/CO_2 source with characteristics representative of a missile plume at an attitude of 20 km. The band model formulation used allowed for the high degree of correlation that exists between the line positions of the source emission spectrum and the atmospheric H_2O/CO_2 absorption spectrum by treating the entire line of sight through the atmosphere and the hot-gas emission source as a single, highly inhomogeneous optical path. Inhomogeneities along the path were accounted for with either the Curtis-Godson (CG) or the Lindquist-Simmons (LS) approximation.

The band model formulation was, however, limited by the assumption that the individual spectral lines within the band could be described by a pressure-broadened Lorentz profile. The effect of this limitation became apparent in subsequent calculations made for hot gas sources that represented missile plumes in the sea level to 60 km altitude range. As the target altitude increased above about 20 km, the computed effective transmittance to space approached unity much more slowly than the transmittance predicted by conventional atmospheric band models. Although a substantial part of the apparent enhancement of the atmospheric absorption is caused by line correlation effects, much of the effect was also attributed to the inappropriateness of using a pressure-broadened Lorentz line shape for such high altitudes.

Typical line widths for pressure broadening in atmospheric applications are of the order $\gamma_L \sim (0.1\ cm^{-1}/atm)\ p$, where p is the total gas pressure. At an altitude of 25 km, the pressure is $p \sim 0.03$ atm, and $\gamma_L \sim 0.003\ cm^{-1}$. For higher altitudes, both p and γ_L are smaller. The mechanism of Doppler

[1] S. J. Young, Band Model Calculations of Atmospheric Transmittance for Hot Gas Line Emission Sources, TR-0075(5647)-1, The Aerospace Corporation, El Segundo, Calif. (31 December 1974).

broadening, on the other hand, is pressure independent* and depends only on the local temperature, the mass of the absorbing or emitting molecule, and the wavelength of the spectral line. For CO_2 in the 2.7-μm region, for example, $\gamma_D \sim 0.003\ cm^{-1}$ throughout the whole atmosphere. Thus, above ~25 km, the use of a pressure-broadened Lorentz line will give a smaller line width (and different shape) than actually exists. Since any atmospheric slant path that extends to space has some portion above 25 km, Doppler broadening should be accounted for. Because of the exponential decrease of pressure and absorber concentration with altitude, most of the radiative transfer effects for an atmospheric path will occur along the low-altitude end. If enough of the path is below 25 km, then the use of a pressure-broadened Lorentz line for the whole path may be justified. It is only for paths that lie totally above ~25 km that Doppler broadening must be accounted for.

Both pressure broadening and Doppler broadening can be accounted for by using the Voigt line shape. This line shape is a convolution of the dispersion (Lorentz) and Gaussian (Doppler) line shapes and reduces to either of these component line shapes in the appropriate temperature and pressure limits. This report is concerned with the use of the Voigt line shape in band model calculations of the effective transmittance of the atmosphere to hot gas line emission sources.

A review of the band model formulation used in the computation of the effective transmittance and the approximation used to incorporate the Voigt line shape are presented in Section II. In Section III, results obtained with the CG and LS approximations are presented, and the limitations of the approximations are discussed. In Section IV, an improved inhomogeneity approximation is formulated, and the results of the formulation are presented.

---

*Collisional narrowing effects on the Doppler line shape and width are not considered here. The whole concept of non-Gaussian shapes and pressure dependence of widths of Doppler lines has only recently[2] been introduced into the field of atmospheric transmittance and absorptance computations.

[2]R. L. Armstrong, "Effect of Collision Narrowing on Atmospheric Transmittance," Appl. Opt. 14, 56 (1975).

II. BAND MODEL FORMULATION

A. FORMULATION FOR LORENTZ AND DOPPLER LINE SHAPES

The band model formulation used here was discussed in detail in earlier reports.[1,3,4] The average radiance in a spectral interval $\Delta\nu$ centered on ν for an optical path that extends from the geometric position s = 0 to s = S is computed from

$$\bar{L}(\nu) = -\int_0^S L^*(\nu, s)\,\frac{d\bar{\tau}(\nu, s)}{ds}\,ds \qquad (1)$$

where $L^*(\nu, s)$ is the Planck radiation function evaluated at wavenumber ν and temperature T(s), and $\bar{\tau}(\nu, s)$ is the mean transmittance for $\Delta\nu$ over the path between s = 0 and the general position s. If more than one absorbing molecular species exists in the path, the total transmittance is assumed to be the product of the transmittances computed for the individual species; i.e., it is assumed that no line correlation exists between the absorption spectra of different species. For the statistical band model formulation in which the number of lines N in $\Delta\nu$ approaches infinity, and for which the assumption is made that the absorption caused by each line whose center occurs in $\Delta\nu$ is confined to $\Delta\nu$, the mean transmittance for a single species is

$$\bar{\tau}(s) = \exp\left(-\frac{\bar{W}(s)}{\delta}\right)$$

---

[3] S. J. Young, Band Model Formulation for Inhomogeneous Optical Paths, TR-0075(5647)-4, The Aerospace Corporation, El Segundo, Calif. (19 December 1974); also, J. Quant. Spectr. Radiative Transfer 15, 483 (1975).

[4] S. J. Young, Addendum to: Band Model Formulation for Inhomogeneous Optical Paths, TR-0076(6970)-3, The Aerospace Corporation, El Segundo, Calif. (31 July 1975).

where $\overline{W}$ is the mean equivalent width of all the lines in $\Delta\nu$, and δ is the mean line spacing parameter $\delta = \Delta\nu / N$. The functional dependence on ν and species is suppressed in Eq. (2) and from here on. Evaluation of the integral of Eq. (1) requires the transmittance derivative, which, from Eq. (2), is

$$\frac{d\overline{\tau}(s)}{ds} = -\overline{\tau}(s)\,\frac{1}{\delta}\,\frac{d\overline{W}(s)}{ds} \tag{3}$$

The mean equivalent width derivative can be written in the form

$$\frac{1}{\delta}\,\frac{d\overline{W}(s)}{ds} = c(s)p(s)\overline{k}(s)y[x(s), \rho(s)] \tag{4}$$

where $c(s)$ and $p(s)$ are the mole fraction of absorber and total pressure distribution, respectively, along the path, and $\overline{k}(s)$ is the mean absorption coefficient band model parameter for the interval $\Delta\nu$ and temperature $T(s)$. The arguments of the function $y(x, \rho)$ are

$$x(s) = \frac{k_e(s)u(s)}{\beta_e(s)} \tag{5}$$

and

$$\rho(s) = \frac{\beta(s)}{\beta_e(s)} \tag{6}$$

where

$$\overline{k}_e(s) = \frac{1}{u(s)} \int_0^s c(s')p(s')\overline{k}(s')ds' \tag{7}$$

and

$$\beta_e(s) = \frac{1}{u(s)\overline{k}_e(s)} \int_0^s c(s')p(s')\overline{k}(s')\beta(s')ds' \tag{8}$$

are path-averaged values of $\overline{k}$ and β, respectively. The parameter x(s) is a measure of optical depth between s = 0 and s, and $\rho(s)$ is a measure of the local inhomogeneity at s. The mean line width to spacing parameter β is defined by

$$\beta_L(s) = 2\pi \frac{\overline{\gamma}_L(s)}{\delta_e(s)} \tag{9a}$$

for Lorentz lines and by

$$\beta_D(s) = \sqrt{\frac{\pi}{\ln 2}} \frac{\overline{\gamma}_D(s)}{\delta_e(s)} \tag{9b}$$

for Doppler lines. In Eq. (9a), $\overline{\gamma}_L(s)$ is the mean Lorentz line width for all the lines in $\Delta\nu$ and for the temperature, pressure, and species concentration conditions at s. In Eq. (9b), $\overline{\gamma}_D(s)$ is the mean Doppler line width for $\Delta\nu$ and the temperature T(s). In either equation, $\delta_e(s)$ is the effective mean line spacing band model parameter for $\Delta\nu$ and temperature T(s). The optical depth is

$$u(s) = \int_0^s c(s')p(s')ds' \tag{10}$$

The functional form of $y(x, \rho)$ depends on the assumed line shape, the assumed distribution of line strengths in $\Delta\nu$, and the approximation used to account for inhomogeneities along the path. Only the exponential-tailed inverse

line strength distribution is considered here. With this limitation, the functional form for the Lorentz line shape within the CG approximation is

$$y(x, \rho) = (2 - \rho)\frac{df(x)}{dx} + (1 - \rho)\frac{f(x)}{x} \tag{11}$$

where

$$f(x) = \frac{1}{\pi}\left(\sqrt{1 + 2\pi x} - 1\right) \tag{12}$$

is the equivalent width curve of growth function. In the LS approximation, the result for the Lorentz line shape is*

$$y(x, \rho) = \frac{2\rho(1 + \pi x) + (1 + \rho^2)\sqrt{1 + 2\pi x}}{\sqrt{1 + 2\pi x}\left(\rho + \sqrt{1 + 2\pi x}\right)^2} \tag{13}$$

The solutions of $y(x, \rho)$ for Doppler lines are not expressible in closed form, but are conveniently obtained by tabular interpolation and approximate solutions. For the LS approximation, the data of Table 1 can be used to obtain $y(x, \rho)$ by interpolation for most practical applications. For small x, the series solution

$$y(x, \rho) = \sum_{n=0}^{\infty} \frac{(-\pi x)^n}{\sqrt{1 + n\rho^2}} \tag{14}$$

---

*The additional factors of π that appear in Eq. (13) [and later in Eq. (17)], but not in Eq. (9) or Eq. (6) of Ref. 4, are included in order to compensate for the form of the band model parameter δ_e used with the band model (Section III).

Table 1. Equivalent Width Derivative Function for an Exponential-Tailed Inverse Intensity Distribution of Doppler Lines in the Lindquist-Simmons Approximation

	ρ						
πx	5.00E-1	1.00E+0	1.25E+0	1.50E+0	2.00E+0	3.00E+0	5.00E+0
1.0E-2	0.99114E+0	0.99299E+0	0.99380E+0	0.99450E+0	0.99556E-0	0.99686E-0	0.99805E-0
2.0E-2	0.98243E+0	0.98608E+0	0.98770E+0	0.98907E+0	0.99119E-0	0.99377E-0	0.99613E-0
5.0E-2	0.95723E+0	0.96603E+0	0.96995E+0	0.97329E+0	0.97844E-0	0.98474E-0	0.99053E-0
1.0E-1	0.91803E+0	0.93460E+0	0.94207E+0	0.94846E+0	0.95836E-0	0.97050E-0	0.98168E-0
2.0E-1	0.84868E+0	0.87828E+0	0.89190E+0	0.90367E+0	0.92200E-0	0.94464E-0	0.96560E-0
5.0E-1	0.69248E+0	0.74750E+0	0.77433E+0	0.79799E+0	0.83553E-0	0.88273E-0	0.92692E-0
1.0E+0	0.53069E+0	0.60490E+0	0.64392E+0	0.67937E+0	0.73706E-0	0.81132E-1	0.88198E-0
2.0E+0	0.36239E+0	0.44564E+0	0.49455E+0	0.54100E+0	0.61957E-0	0.72444E-0	0.82669E-0
5.0E+0	0.18622E+0	0.25945E+0	0.31182E+0	0.36593E+0	0.46452E-0	0.60548E-0	0.74932E-0
1.0E+1	0.10301E+0	0.15883E+0	0.20643E+0	0.25986E+0	0.36450E-0	0.52442E-1	0.69490E-0
2.0E+1	0.54426E-1	0.92598E-1	0.13195E+0	0.18053E+0	0.28411E-0	0.45506E-0	0.64664E-0
5.0E+1	0.22544E-1	0.43173E-1	0.70728E-1	0.10995E+0	0.20490E-0	0.38046E-0	0.59211E-0
1.0E+2	0.11408E-1	0.23642E-1	0.43542E-1	0.75384E-1	0.16102E-0	0.33469E-0	0.55672E-0
2.0E+2	0.57384E-2	0.12759E-1	0.26649E-1	0.51787E-1	0.12735E-0	0.29611E-0	0.52535E-0
5.0E+2	0.23038E-2	0.55566E-2	0.13871E-1	0.31709E-1	0.94277E-1	0.25368E-0	0.48873E-0
1.0E+3	0.11533E-2	0.29368E-2	0.84594E-2	0.21992E-1	0.75569E-1	0.22668E-0	0.46396E-0
2.0E+3	0.57700E-3	0.15432E-2	0.51628E-2	0.15322E-1	0.60853E-1	0.20319E-0	0.44126E-0
5.0E+3	0.23088E-3	0.65458E-3	0.26937E-2	0.95640E-2	0.45971E-1	0.17650E-0	0.41390E-0
1.0E+4	0.11546E-3	0.34067E-3	0.16503E-2	0.67263E-2	0.37322E-1	0.15906E-0	0.39491E-0
2.0E+4	0.57731E-4	0.17676E-3	0.10132E-2	0.47468E-2	0.30380E-1	0.14358E-0	0.37718E-0
5.0E+4	0.23093E-4	0.73960E-4	0.53344E-3	0.30083E-2	0.23224E-1	0.12570E-0	0.35546E-0
1.0E+5	0.11547E-4	0.38163E-4	0.32916E-3	0.21370E-2	0.18996E-1	0.11383E-0	0.34018E-0

is convenient, whereas, for $\rho \lesssim 0.5$, the approximation

$$y(x, \rho) \simeq \frac{2}{\left\{(1 + \pi x)[1 - \pi x(\rho^2 - 1)]\right\}^{1/2}} \tag{15}$$

is accurate to better than 1 percent. In the CG approximation, $y(x, \rho)$ is defined by

$$y(x, \rho) = (2 - \rho)\frac{dH(x)}{dx} + (1 - \rho)\frac{H(x)}{x} \tag{16}$$

where

$$H(x) = \frac{2}{\pi^{3/2}} \int_0^\infty \ln \left[1 + \pi x e^{-z^2}\right] dz \tag{17}$$

is the equivalent width curve of growth function for Doppler lines and the exponential-tailed inverse line strength distribution. For small x

$$H(x) \simeq \frac{1}{\pi} \sum_{n=0}^{\infty} \frac{(-\pi x)^{n+1}}{(n + 1)^{3/2}} \tag{18}$$

whereas, for large x

$$H(x) \simeq \frac{4}{3\pi^{3/2}} (\ln \pi x)^{3/2} \left[1 + \frac{\pi^2/8}{(\ln \pi x)^2} + \frac{7\pi^4/640}{(\ln \pi x)^4}\right] \tag{19}$$

For intermediate x, H(x) can be interpolated from the data of Table 2. The derivative $dH(x)/dx$ may be determined by differentiating Eqs. (18) and (19) or by performing a numerical differentiation of the data in Table 2. In practice,

Table 2. Curve-of-Growth Function for Doppler Line Shape and Exponential-Tailed Inverse Line Strength Distribution

πx	$\pi H(x)$
0.1	0.09665
0.2	0.18722
0.4	0.35325
0.6	0.50289
0.8	0.63940
1.0	0.76515
2.0	1.28138
4.0	2.00567
6.0	2.52794
8.0	2.94136
10	3.28568
20	4.47964
40	5.84661
60	6.71916
80	7.36866
100	7.88910
200	9.59377
400	11.4233
600	12.5478
800	13.3689
1000	14.0187

it is more convenient to obtain $dH(x)/dx$ for intermediate x from the data of Table 1 by interpolating on the $\rho = 1$ column. This is possible because, for $\rho = 1$, i.e., for a homogeneous path, the CG and LS solutions for $y(x, 1)$ are identical, and for either

$$y(x, 1) = \frac{dH(x)}{dx} \tag{20}$$

The equivalent width factor of Eq. (3) is given by Eqs. (4) through (20). The transmittance factor of Eq. (3) is given by Eq. (2), where, for the CG approximation

$$\frac{\overline{W}(s)}{\delta} = \beta_e(s) f[x(s)] \tag{21a}$$

for Lorentz lines and

$$\frac{\overline{W}(s)}{\delta} = \beta_e(s)\, H[x(s)] \tag{21b}$$

for Doppler lines. In the LS approximation, $\overline{W}(s)/\delta$ must be integrated from the derivative function

$$\frac{\overline{W}(s)}{\delta} = \int_0^s \frac{1}{\delta} \frac{d\overline{W}(s')}{ds}\, ds' \tag{22}$$

for either line shape.

The formal representation of the statistical band model method for computing the radiance of inhomogeneous optical paths is given by Eqs. (1) through (22) for Lorentz or Doppler line shape in either the CG or LS approximation. Some comments are now given concerning the application of the model to the present problem, where the optical path is composed of two distinct component paths. Let the path position $s = 0$ represent the point where the spectral

radiance is being measured. (For a space sensor geometry, $s = 0$ is the altitude above which the atmosphere is assumed to be nonabsorbing.) Let $s = s_0$ be the boundary between the atmosphere and the near (to the sensor) boundary of the hot gas source, and $s = S$ represent the far boundary of the source. If Eq. (1) is written as the sum of integrals from $s = 0$ to s_0 and from s_0 to S, then the first term represents the atmospheric contribution to the measured radiance, and the second term represents the hot gas source contribution to the radiance with allowance made for absorption by the intervening atmosphere. All results presented here are for the 2.7-μm region, and, for the target plume temperatures used, the atmospheric contribution to the total radiance can be neglected. The second term

$$\bar{L} = -\int_{s_0}^{S} L^*(s) \frac{d\bar{\tau}(s)}{ds}\, ds \tag{23}$$

also represents the unattenuated radiance of the source if the intervening atmosphere is nonabsorbing. The effective transmittance of the atmosphere is computed by taking the ratio of the solution of Eq. (23) for the absorbing atmosphere case to the solution for the nonabsorbing case, and is designated $\bar{\tau}_e$. Because this method of computing transmittance implicity takes line correlation into account, $\bar{\tau}_e$ will always be smaller than the transmittance $\bar{\tau}$ computed from Eqs. (2) and (21), or (22), with $s = s_0$.

The two conditions for which Eq. (23) must be evaluated are conveniently accommodated by writing $u(s)$, $\bar{k}_e(s)$, and $\beta_e(s)$ for $s \geq s_0$ as

$$u(s) = u(s_0) + \int_{s_0}^{s} c(s')p(s')ds' \tag{24}$$

$$\bar{k}_e(s) = \frac{1}{u(s)}\left[u(s_0)\bar{k}_e(s_0) + \int_{s_0}^{s} c(s')p(s')\bar{k}(s')ds'\right] \tag{25}$$

and

$$\beta_e(s) = \frac{1}{u(s)\bar{k}_e(s)}\left[u(s_0)\bar{k}_e(s_0)\beta_e(s_0) + \int_{s_0}^{s} c(s')p(s')\bar{k}(s')\beta(s')ds'\right] \tag{26}$$

For the computation of the radiance value that includes atmospheric absorption, $u(s_0)$, $\bar{k}_e(s_0)$, and $\beta_e(s_0)$ are computed from Eqs. (10), (7), and (8), respectively, for the whole atmospheric path by using $s = s_0$ as the upper integration limit. For the computation of the unattenuated source radiance, $u(s_0)$ is simply set to zero. This corresponds to using $c(s') = 0$ in Eq. (10) and represents a nonabsorbing atmospheric path.

B. EXACT FORMULATION FOR VOIGT LINE SHAPE

Formal solutions for the equivalent width derivative functions can be obtained for the Voigt line shape by the same procedures used earlier for the Lorentz and Doppler lines.[3,4] One has only to carry through the development with the spectral absorption coefficient for the Voigt line

$$k(\nu, s) = \sqrt{\frac{\ln 2}{\pi}}\,\frac{S(s)}{\gamma_D(s)}\,K[a(s),\ w(s)] \tag{27}$$

where S(s) is the line strength, a(s) is a measure of the local Lorentz line width to Doppler line width

$$a(s) = \sqrt{\ln 2}\,\frac{\gamma_L(s)}{\gamma_D(s)} \tag{28}$$

w(s) is the measure of spectral displacement from the line center ν_0

$$w(s) = \sqrt{\ln 2}\,\frac{\nu - \nu_0}{\gamma_D(s)} \tag{29}$$

and K(a, w) is the line profile function

$$K(a, w) = \frac{a}{\pi}\int_{-\infty}^{\infty} \frac{e^{-u^2}}{a^2 + (w - u)^2}\,du \tag{30}$$

The result for an isolated Voigt line is

$$\frac{dW(s)}{ds} = c(s)p(s)S(s)y[x(s),\ a(s),\ \rho_L(s),\ \rho_D(s)] \tag{31}$$

where

$$y(x, a, \rho_L, \rho_D) = \frac{2}{\sqrt{\pi}}\int_0^{\infty} K(a, z)e^{-xK(a\rho_D/\rho_L,\ z\rho_D)}\,dz \tag{32}$$

The arguments of y are

$$x(s) = \sqrt{\frac{\ln 2}{\pi}}\,\frac{S_e(s)u(s)}{\gamma_{eD}(s)} \tag{33}$$

$$\rho_L(s) = \frac{\gamma_L(s)}{\gamma_{eL}(s)} \tag{34}$$

and

$$\rho_D(s) = \frac{\gamma_D(s)}{\gamma_{eD}(s)} \tag{35}$$

with a(s) given by Eq. (28). Note that the Doppler dimensionless optical depth is used. The path-averaged parameters $S_e(s)$, $\gamma_{eL}(s)$, and $\gamma_{eD}(s)$ were defined earlier. For a band of equal intensity Voigt lines

$$\frac{1}{\delta}\frac{d\overline{W}(s)}{ds} = c(s)p(s)\overline{k}(s)y[x(s),\ a(s),\ \rho_L(s),\ \rho_D(s)] \tag{36}$$

where y is the same function as for an isolated line, Eq. (32), with the x and ρ arguments defined by Eqs. (5) and (6), respectively, and a(s) by

$$a(s) = \frac{1}{2\sqrt{\pi}}\frac{\beta_L(s)}{\beta_D(s)} \tag{37}$$

For a band of lines with an exponential or exponential-tailed inverse line strength distribution, the mean equivalent width derivative is given by Eq. (36), but the derivative function y is given by

$$y(x, a, \rho_D, \rho_L) = \frac{2}{\sqrt{\pi}}\int_0^\infty \frac{K(a,\ z)}{[1 + xK(a\rho_D/\rho_L,\ z\rho_D)]^n}\,dz \tag{38}$$

with n = 2 for the exponential distribution and n = 1 for the exponential-tailed inverse distribution.

None of the expressions for y given by Eqs. (32) and (38) is amenable to a closed-form solution. For the pure Doppler line shape, solutions were obtained by compiling tables of y with respect to the two independent variables x and ρ from which y could be obtained by interpolation. For the Voigt line

shape, however, there are four independent variables, and the tabular approach is not practical. The solution used here is to approximate the equivalent width of a Voigt line by a combination of the component Lorentz and Doppler equivalent widths.

C. APPROXIMATE FORMULATION FOR VOIGT LINE SHAPE

The Voigt profile is complex enough that, even for homogeneous paths, simple solutions for the equivalent width of an isolated line have not been formulated. The equivalent width is either computed numerically as needed, interpolated from tables of equivalent width versus a and x, or computed from approximate expressions. An example of available interpolation tables has been given by Jansson and Korb.[5] Three methods of approximating the equivalent width have been discussed by Hansen and McKenzie,[6] Yamada,[7] and Rogers and Williams,[8] respectively. The method of Hansen and McKenzie approximates W(a,x) directly in terms of a and x. Yamada's approach takes W to be the Lorentz or Doppler equivalent width in the limits of strong and weak absorption, respectively, and gives the solution in the transition region as one or the other of these equivalent widths modified by a function of a and x. Of the three approximations, that of Rodgers and Williams is the simplest to implement and also the most accurate. For a homogeneous path and isolated Voigt line, their representation for W is

---

[5] P. A. Jansson and C. L. Korb, "A Table of the Equivalent Width of Isolated Lines with Combined Doppler and Collision Broadened Profiles," J. Quant. Spectr. Radiative Transfer 8, 1399 (1968).

[6] C. F. Hansen and R. L. McKenzie, "Analytic Approximations for Curves of Growth of Doppler-Lorentz Broadened Lines," J. Quant. Spectr. Radiative Transfer 11, 349 (1971).

[7] H. Y. Yamada, "Total Radiances and Equivalent Widths of Isolated Lines with Combined Doppler and Collision Broadened Profiles," J. Quant. Spectr. Radiative Transfer 8, 1463 (1968).

[8] C. D. Rodgers and A. P. Williams, "Integrated Absorption of a Spectral Line with the Voigt Profile," J. Quant. Spectr. Radiative Transfer 14, 319 (1974).

$$W = \left[W_L^2 + W_D^2 - \left(\frac{W_L W_D}{W_W} \right)^2 \right]^{1/2} \tag{39}$$

where W_L and W_D are the equivalent widths that would result if the line shape were assumed to be purely Lorentz and Doppler, respectively, and W_W is the weak-limit form for the equivalent width of any line shape

$$W_W = Su \tag{40}$$

The reported maximum error of the approximation is ~8 percent and occurs for x (the Doppler depth) $\simeq 1$ when $a \simeq 0.47$ and along the curve $ax \simeq 15$ when $a \lesssim 0.00083$ ($x \gtrsim 1.8 \times 10^4$).

This approximation is used here for bands of lines and inhomogeneous optical paths as follows. The mean equivalent widths $\overline{W}_L(s)/\delta$ and $\overline{W}_D(s)/\delta$ are computed in either the CG or LS approximations according to Eqs. (21) or (22) and are combined according to the algebraic form of Eq. (39) in order to obtain $\overline{W}(s)/\delta$. The weak-limit form is taken as

$$\frac{\overline{W}_W(s)}{\delta} = u(s)\overline{k}_e(s) \tag{41}$$

The result for $\overline{W}(s)/\delta$ is then used in Eq. (2) to obtain the transmittance $\overline{\tau}(s)$. The derivative of the mean equivalent width could be obtained by a numerical differentiation of $\overline{W}(s)/\delta$, but is obtained in practice by differentiating Eq. (39) analytically to obtain the derivative function

$$y(x, a, \rho_D, \rho_L) = Ay_L(x/2a\sqrt{\pi}, \rho_L) + By_D(x, \rho_D) + C \tag{42}$$

where y_L and y_D are the Lorentz and Doppler derivative functions, respectively. The coefficients of Eq. (42) are

$$A = \frac{\overline{W}_L/\delta}{\overline{W}/\delta}\left\{1 - \left(\frac{\overline{W}_D/\delta}{\overline{W}_W/\delta}\right)^2\right\} \tag{43}$$

$$B = \frac{\overline{W}_D/\delta}{\overline{W}/\delta}\left\{1 - \left(\frac{\overline{W}_L/\delta}{\overline{W}_W/\delta}\right)^2\right\} \tag{44}$$

$$C = \frac{\overline{W}_W/\delta}{\overline{W}/\delta}\left(\frac{\overline{W}_L/\delta}{\overline{W}_W/\delta}\right)^2\left(\frac{\overline{W}_D/\delta}{\overline{W}_W/\delta}\right)^2 \tag{45}$$

The dimensionless optical depth x is taken as the Doppler depth. With this result for y, the mean equivalent width derivative is computed from Eq. (4) and the transmittance derivative from Eq. (3).

The main assumptions made in this use of the Rodgers and Williams approximation is that the mean equivalent widths for arrays of Lorentz and Doppler lines combine in the same way as the equivalent widths of isolated lines. Since the curve-of-growth functions for bands of Lorentz lines do not differ greatly from that for an isolated line regardless of the line intensity distribution used (and similarly for the Doppler case), this assumption should not be too inaccurate.

Note that the functional form of Eq. (39) always yields $\overline{W}/\delta \geq \overline{W}_L/\delta$, $\overline{W}/\delta \geq \overline{W}_D/\delta$. Consequently, the transmittance $\overline{\tau}$ computed by Eq. (2) for the Voigt line shape is always less than or equal to the transmittance computed for the pure Lorentz or Doppler line shape. This result is not necessarily true for the effective transmittance $\overline{\tau}_e$.

III. RESULTS WITH THE CG AND LS INHOMOGENEITY APPROXIMATIONS

A. CALCULATION CONDITIONS AND DATA

The band model formulation of Section II is complete, but its use requires specification of the pressure, temperature, and species concentration (pTc) variations along the atmospheric and source portions of the optical path and specification of the fundamental band model parameters $\overline{k}$, δ_e, and $\overline{\gamma}$.

The pTc variation along the atmospheric path was interpolated from the altitude profiles tabulated by McClatchey et al.[9] for five model atmospheres. For all of the results presented here, the tropical model atmosphere was used. The profiles for this atmosphere are plotted in Fig. 1 The line-of-sight viewing geometry consists of a space sensor looking down through the atmosphere at a hot gas plume emission source at some altitude between 0 and 60 km. The zenith angle from the target to sensor is 75 deg.

The plume model used is given in Table 3. The model assumes a homogeneous and isothermal hot gas exhaust contained in an axisymmetric cylindrical volume. The pTc properties and dimensions of the cylinder are allowed to vary with altitude in order to simulate the plume properties of a real missile. All of the results obtained here pertain to a single line of sight that intersects this plume at right angles to the plume axis and passes through a full diameter of the plume. The source portion of the total path is thus a homogeneous and isothermal path segment.

---

[9] R. A. McClatchey, R. W. Fenn, J. E. A. Selby, F. E. Volz, and J. S. Garing, Optical Properties of the Atmosphere (Revised), AFCRL-71-0279, Air Force Cambridge Research Laboratory, Bedford, Mass. (10 May 1971).

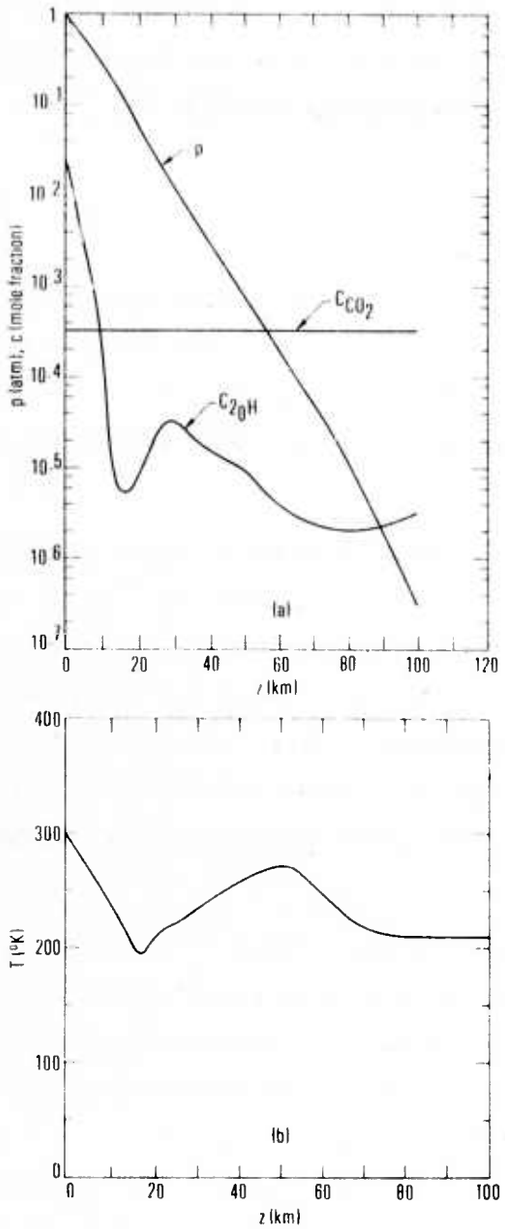

Figure 1. Tropical Model Atmosphere (derived from data of Ref. 9). (a) Altitude profiles for pressure and species concentrations; (b) Altitude profile for temperature.

Table 3. Homogeneous and Isothermal Plume Model

z, km	r, m	L, m	T, °K
0	1.488	16.21	2207.0
5	1.718	37.64	1867.4
10	2.170	71.35	1625.2
15	2.870	133.9	1417.8
20	3.865	237.9	1249.4
25	5.197	409.5	1105.1
30	6.897	704.1	975.8
35	8.918	1.260×10^3	844.4
40	11.29	2.237×10^3	723.5
45	14.09	3.789×10^3	622.5
50	17.54	5.944×10^3	545.6
55	22.46	9.817×10^3	478.7
60	29.41	1.444×10^4	441.5

z = source altitude; r = plume radius; L = plume length; T = plume temperature. The plume gas pressure is the ambient pressure at altitude z. The mole fraction of H_2O is 0.2533 for all z. The mole fraction of CO_2 is 0.03714 for all z.

The band model parameters used here were discussed in detail in an earlier report.[10] For both CO_2 and H_2O, the parameters represent a combining of band model parameters derived from the comprehensive atmospheric

[10] S. J. Young, Band Model Parameters for the 2.7-μm Bands of H_2O and CO_2 in the 100 to 300°K Temperature Range, TR-0076(6970)-4, The Aerospace Corporation, El Segundo, Calif. (31 July 1975).

absorption line data compilation of AFCRL[11] and band model parameters tabulated in the NASA Handbook of Infrared Radiation from Combustion Gases.[12] The former band model parameters were used to represent the low-temperature variation of the final parameter set; the latter represent the high-temperature variation. For intermediate temperatures, the parameters of the final set were interpolated from transition curves drawn from one of the component sets to the other. For both CO_2 and H_2O, the final parameter sets display a smooth and consistent variation of the parameters from temperatures as low as 100 to as high as 3000°K. The sets cover the entire 2.7-μm bands of H_2O and CO_2 and were constructed to represent a spectral resolution of 25 cm^{-1}.

The line spacing parameter of the final set is consistent for use with the statistical band model for a constant line intensity distribution. For other distributions, δ_e must be multiplied by an appropriate constant or this constant must be incorporated in the equations of the band model formulation. The latter approach is taken here and explains the factors of π (the appropriate constant for the exponential-tailed inverse line strength distribution) that occur at various places throughout the discussion of Section II (and later in Section IV).

Most of the results presented here are for the transmittance $\bar{\tau}$ and the effective transmittance $\bar{\tau}_e$ (each computed with 25 cm^{-1} resolution) appropriately averaged over three wide bandpasses in the 2.7-μm region. The regions were selected to represent the low wavenumber wing (3350-3575 cm^{-1}),

---

[11] R. A. McClatchey, W. S. Bendect, S. A. Clough, D. E. Burch, R. F. Calfee, K. Fox, L. S. Rothman, and J. S. Garing, AFCRL Atmospheric Absorption Line Parameters Compilation, AFCRL TR-73-00096, Air Force Cambridge Research Laboratory, Bedford, Mass. (26 January 1973).

[12] C. B. Ludwig, W. Malkmus, J. E. Reardon, and J. A. L. Thomson, Handbook of Infrared Radiation from Combustion Gases, NASA SP-3080, eds. R. Goulard and J. A. L. Thompson (1973).

the bandcenter (3575-3725 cm^{-1}), and the high wavenumber wing (3725-3950 cm^{-1}) of the combined H_2O/CO_2 vibration band. Radiative transfer effects in the latter spectral region are dominated by H_2O. If ν_1 and ν_2 represent the lower and upper wavenumber limits, respectively, of one of these bandpasses, the average transmittances for $\overline{\tau}$ and $\overline{\tau}_e$ are computed from

$$T = \frac{1}{\nu_2 - \nu_1} \int_{\nu_1}^{\nu_2} \overline{\tau}(\nu)\, d\nu \tag{46}$$

and

$$T_e = \frac{\int_{\nu_1}^{\nu_2} \overline{L}_a(\nu)\, d\nu}{\int_{\nu_1}^{\nu_2} \overline{L}_u(\nu)\, d\nu} \tag{47}$$

where $\overline{L}_a(\nu)$ and $\overline{L}_u(\nu)$ are the 25 cm^{-1} resolution solutions of Eq. (23) for the cases where the intervening atmosphere is and is not absorbing, respectively. Since $\overline{L}_a(\nu) = \overline{\tau}_e(\nu)\, \overline{L}_u(\nu)$ by definition, the form of Eq. (47) reduces to that of Eq. (46) if $\overline{L}_u(\nu)$ is constant across the bandpass.

B. RESULTS AND DISCUSSIONS

Bandpass averaged results for T versus altitude are shown in Fig. 2. For all three bandpasses, the curve for the Voigt line shape makes a smooth transition from the Lorentz curve to the Doppler curve in the altitude region from 15 to 40 km. The spectral variations of $\overline{\tau}$ (25 cm^{-1} resolution) for the altitude z = 35 km and for each line shape are shown in Fig. 3, where it is shown that, at all spectral positions, the absorption caused by the Voigt line shape is the greatest.

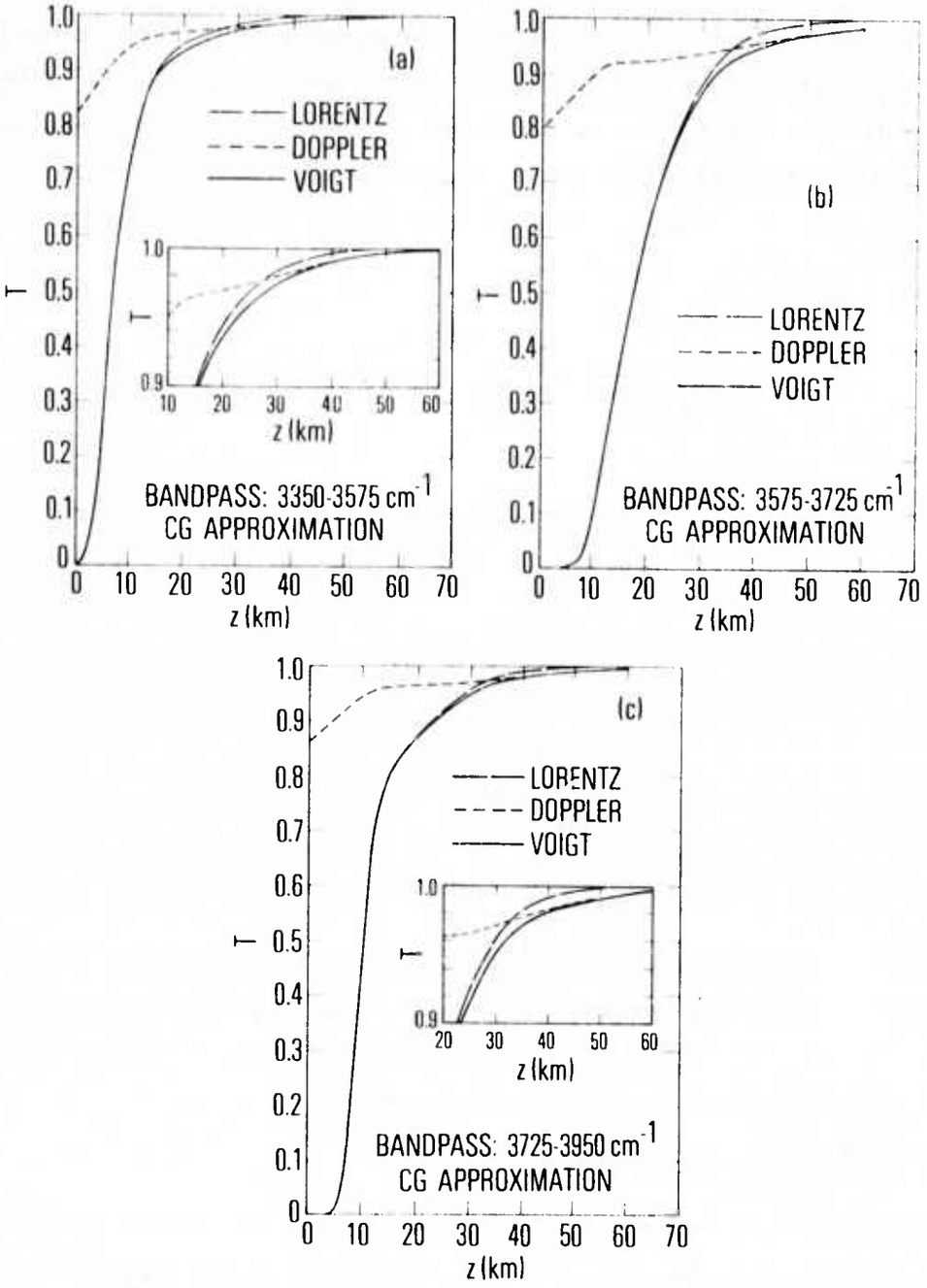

Figure 2. Altitude Variation of T Computed for the Lorentz, Doppler, and Voigt Line Shapes and with the CG Approximation. (a) 3350-3575 cm^{-1} bandpass; (b) 3575-3725 cm^{-1} bandpass; (c) 3725-3950 cm^{-1} bandpass.

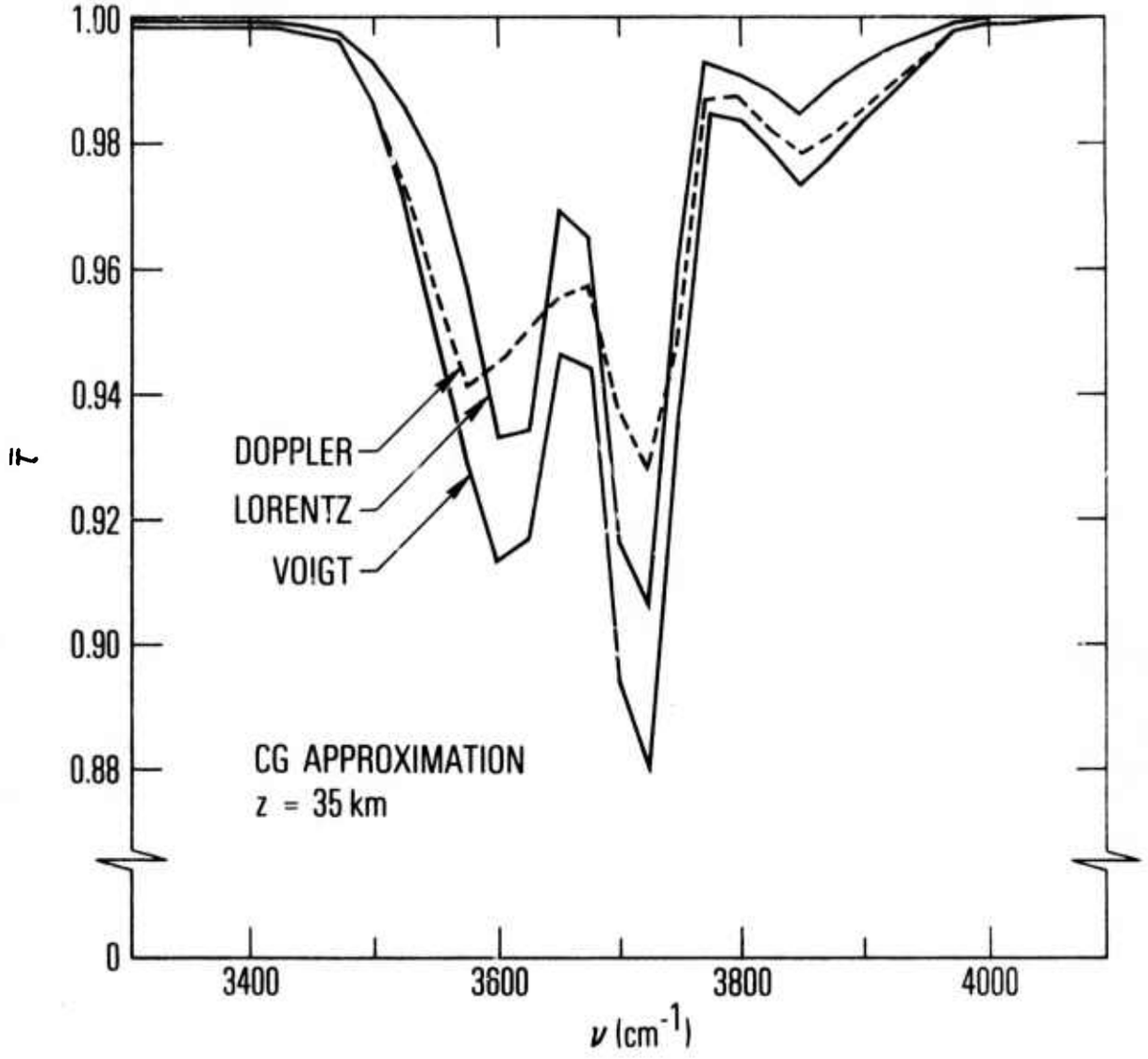

Figure 3. Spectral Variation of $\bar{\tau}(\nu)$ at z = 35 km Computed for the Lorentz, Doppler, and Voigt Line Shapes and with the CG Approximation

All of the results of Figs. 2 and 3 were obtained by using the CG approximation. The results obtained with the LS approximation were nearly the same as with the CG approximation. The largest difference in the result for T computed with the two approximations was ~ 60 percent, but this occurred for the center bandpass (strongest absorbing region) and $z = 0$, where $\bar{\tau}$ was $\sim 2.4 \times 10^{-20}$. The largest difference for a transmittance value large enough to be meaningful was ~ 7 percent and occurred for the center bandpass with $z = 10$ km. The transmittance value was ~ 0.08. Above ~ 15 km, the difference in results obtained with the CG and LS approximations was ≤ 1 percent, and the transmittances were all > 0.3. These results reinforce the hypothesis that the degree of inhomogeneity encountered along a strictly atmospheric slant path is not too large to be adequately handled by the CG approximation.

Bandpass averaged results for T_e versus target source altitude are shown in Figs. 4 and 5 for calculations made with the CG and LS approximations, respectively. Comparison of results is facilitated by discussing the results for each line shape individually. Consider first the Lorentz line shape results. The failing of the CG approximation for highly inhomogeneous optical paths and Lorentz line shape has been shown to result in computed values for $\bar{\tau}_e(\nu)$ that are too large at some spectral positions;[1] so large, in fact, that frequently $\bar{\tau}_e(\nu)$ is not only greater than $\bar{\tau}(\nu)$, but also greater than unity. These errors occurred in regions of weak absorption, such as the band wings. An example of this failing is demonstrated in Fig. 6a for the altitude $z = 15$ km. The LS approximation was devised to correct this discrepancy, and the result of Fig. 6b displays its success. Although $\bar{\tau}_e(\nu) > 1$ for some ν in the CG approximation, the extent of the error is not large enough to make itself felt in the bandpass averages T_e. The Lorentz line results for T_e in Fig. 4 are all less than unity. They are, however, greater than the LS results of Fig. 5 in every case.

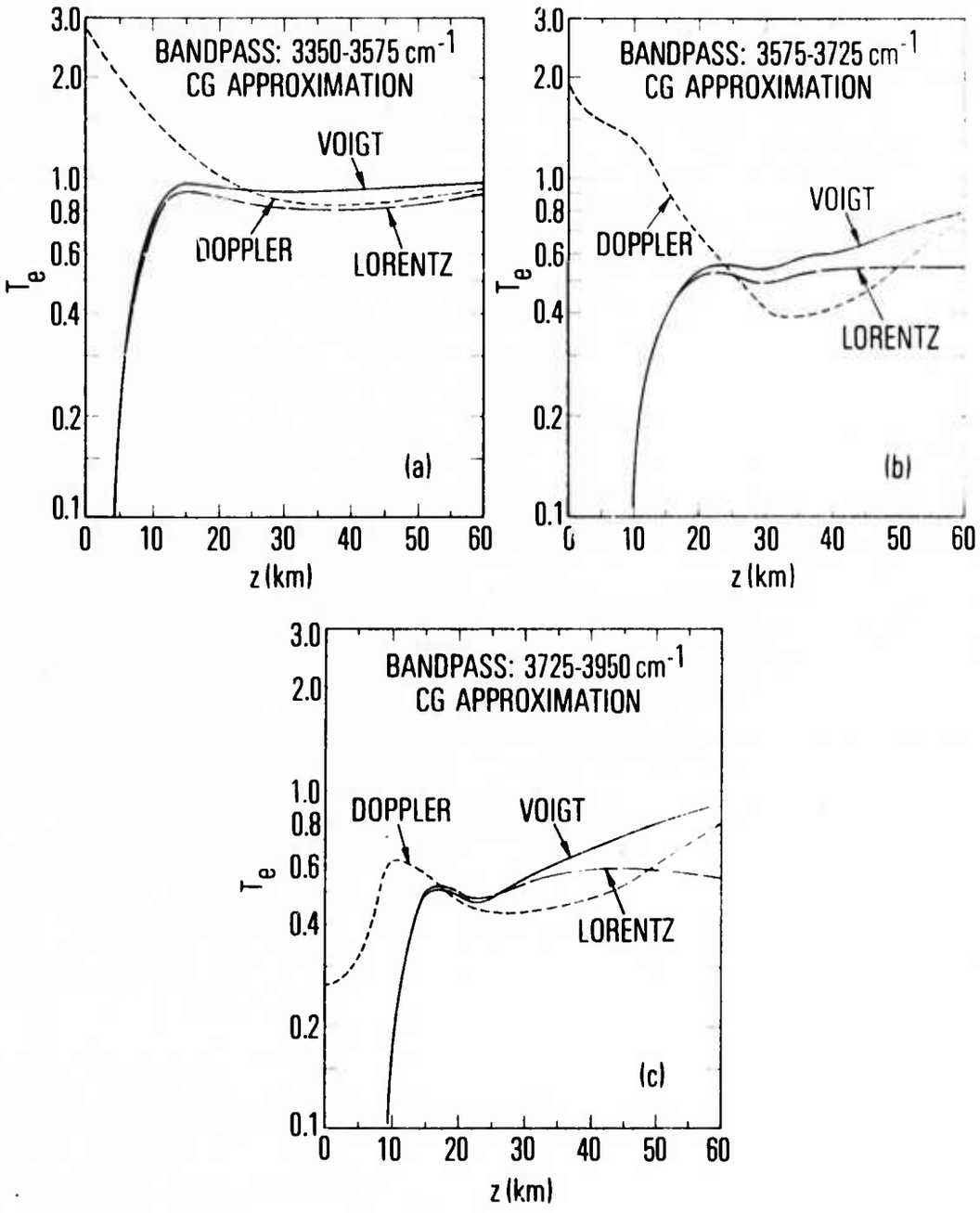

Figure 4. Altitude Variation of T_e Computed for the Lorentz, Doppler, and Voigt Line Shapes and with the CG Approximation. (a) 3350-3575 cm^{-1} bandpass; (b) 3575-3725 cm^{-1} bandpass; (c) 3725-3950 cm^{-1} bandpass.

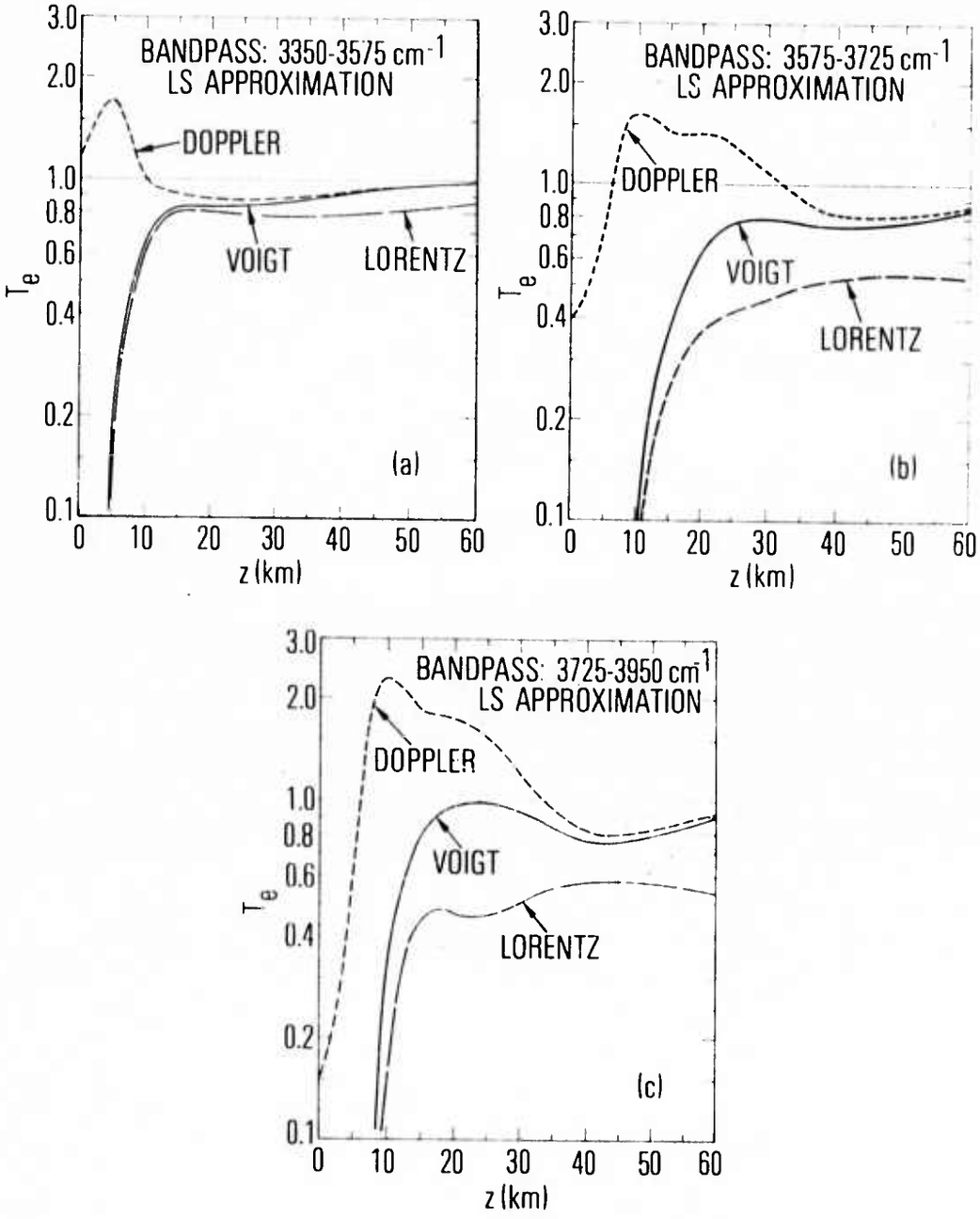

Figure 5. Altitude Variation of T_e Computed for the Lorentz, Doppler, and Voigt Line Shapes and with the LS Approximation. (a) 3350-3575 cm^{-1} bandpass; (b) 357503725 cm^{-1} bandpass; (c) 3725-3950 cm^{-1} bandpass.

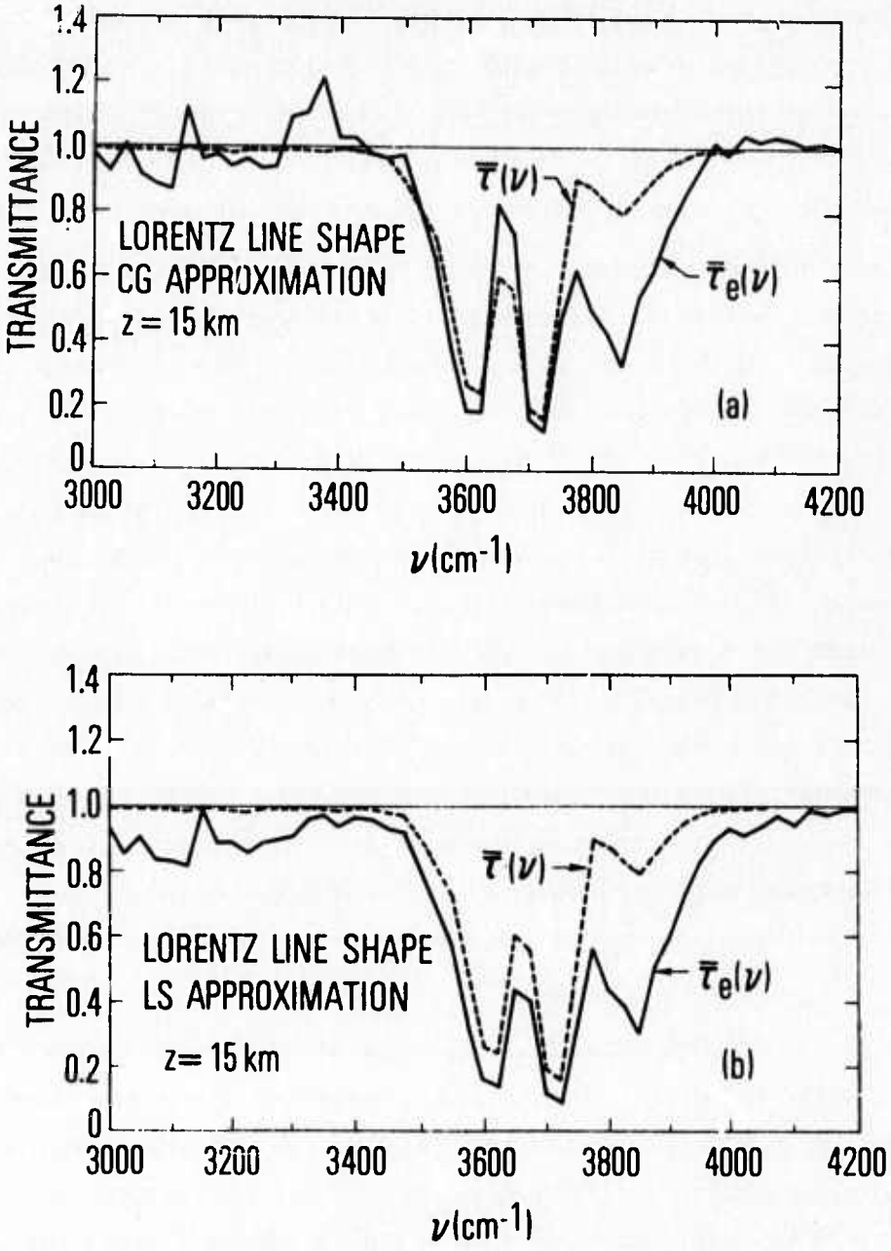

Figure 6. Spectral Variation of $\overline{\tau}_e(\nu)$ at z = 15 km Computed for the Lorentz Line Shape. (a) CG approximation [$\overline{\tau}_e(\nu)$ is not physically meaningful whenever it is greater than $\overline{\tau}(\nu)$]; (b) LS approximation.

In almost every case of Figs. 4 and 5, the result for T_e obtained for the pure Lorentz line shape increases with z up to ~ 15 to 20 km, and then maintains a value much less than unity as z is increased further. This effect was mentioned in the Introduction and is a result of using the pressure-broadened Lorentz line shape in an altitude region where its use is not valid.

The T_e results for the Doppler line shape computed with the CG approximation are shown in Fig. 4. As for the Lorentz line shape, $\bar{\tau}_e(\nu)$ computed with this approximation can be greater than unity. Now, however, the seriousness of the error is so great that even the bandpass averages can exceed unity. For the 3350 to 3575 cm^{-1} bandpass (Fig. 4a), T_e begins to approach a realistic variation with altitude at $z \simeq 30$ km. For the other two bandpasses, a realistic variation is not yet achieved, even at z = 60 km. For the Lorentz line case, the LS approximation was able to give significantly more realistic results for $\bar{\tau}_e(\nu)$ than did the CG approximation. The results of Fig. 5 indicate that, for Doppler lines, the LS approximation gives only little improvement over the CG approximation. Values of $T_e > 1$ occur for each of the bandpasses. The slight improvement provided by the LS approximation is that the variation of T_e with altitude becomes reasonable at a lower altitude. For the low wavenumber bandpass, the variation is reasonable above $z \simeq 20$ km. For the other two bandpasses, the variation is reasonable above $z \simeq 40$ km.

The results for T_e obtained for the Voigt line shape are also shown in Figs. 4 and 5. Because the calculations for the Voigt line shape are carried out with the results for the pure Lorentz and Doppler line shapes, and because the Doppler component results for both the CG and LS approximations are unrealistic, the results for the Voigt line shape do not have much meaning. Some interesting features should be mentioned however. The Voigt results for T_e computed with the LS approximation always lie between the T_e curves computed for the Lorentz and Doppler line shape. With the CG approximation, on the other hand, this behavior is not obtained. In fact, the results obtained with the CG approximation display a surprisingly realistic

variation for T_e computed for the Voigt line shape despite the unreasonableness of the component line shape results. The behavior of neither the CG nor the LS approximations follows that required for T; viz., that the Voigt result for T be smaller than either of the component line shape results.

In the next section, the failure of the LS approximation when used with the Doppler line shape is discussed, and a new approximation is formulated to account for inhomogeneities along an optical path.

IV. THE TWO-PATH DERIVATIVE APPROXIMATION

A. INTRODUCTION

In order to understand the fundamental reasons for the failure of the LS approximation when applied to the Doppler line shape, consider the simplified problem of two homogeneous path segments in series. The first lies between $s = 0$ and $s = s_0$ and has optical and thermodynamic properties identified by subscript 1; the second lies between $s = s_0$ and $s = S$ and has properties identified by subscript 2. Two effects must be considered: the change in line width as s traverses from the first path segment into the second, and the change in line density for the same transition. Consider first an isolated line, and in order to simplify the problem even further, assume the line to be rectangular in shape. The variation of the line width with s is

$$\gamma(s) = \begin{cases} \gamma_1 & 0 \leq s \leq s_0 \\ \gamma_2 & s_0 < s \leq S \end{cases} \tag{48}$$

Assume that $\gamma_2 > \gamma_1$. (As an approximation for Doppler lines, $\gamma_2 > \gamma_1$ implies that the temperature relation for the two paths is $T_2 > T_1$. For Lorentz lines, $\gamma_2 > \gamma_1$ would occur, for example, if the pressure relation were $p_2 > p_1$ when all the other properties of the two path segments were equal.) The variation of the path-averaged line width with s is

$$\gamma_e(s) = \begin{cases} \gamma_1 & 0 < s \leq s_0 \\ \dfrac{c_1 p_1 \gamma_1 S_1 s_0 + c_2 p_2 \gamma_2 S_2 (s - s_0)}{c_1 p_1 S_1 s_0 + c_2 p_2 S_2 (s - s_0)} & s_0 < s \leq S \end{cases} \tag{49}$$

The variations of $\gamma(s)$ and $\gamma_e(s)$ are shown schematically in Fig. 7 for a rectangular line centered on ν_0. In the LS approximation, the contribution to the radiance at $s = 0$ from a path element ds at s is obtained by assuming that the emission line width in ds is $\gamma(s)$, and that the radiation from ds is attenuated by a homogeneous path between $s = 0$ and s along which the absorption line has the constant value $\gamma_e(s)$. As is evident from Fig. 7, when $s > s_0$, $\gamma_e(s) < \gamma(s)$. Consequently, the radiation emitted in ds from any spectral element $d\nu$ in the line wings beyond $|\nu - \nu_0| = \gamma_e(s)$ is not attentuated at all in traversing the path to $s = 0$. If the path properties are such that $\gamma_2 \gg \nu_1$, and the path-averaged line width $\gamma_e(s)$ is so heavily weighted by the properties of region 1 that $\gamma_e(s) \simeq \gamma_1$, even for $s >> s_0$, a substantial part of the radiation from region 2 will arrive at $s = 0$ without being attenuated. On the other hand, when the radiance at $s = 0$ due to the second region alone is computed, no consideration is given to region 1, and $\gamma_e(s)$ has the constant value $\gamma_e(s) = \gamma_2$ for all $s > s_0$. In this case, the radiation from each spectral interval $d\nu$ of ds is properly attenuated as it traverses toward $s = 0$. The net effect is that a larger radiance is computed for the total path, which consists of regions 1 and 2 in series, than is computed for region 2 alone. This result is totally unacceptable. For real spectral line shapes, the wing radiation from the emission line is not completely unattenuated in the total path radiance calculation, but can be significantly underestimated because of this effect.

The consideration of the change in line density between the two regions is similar to that for the line width. Assume that $\bar{\gamma}_1 = \bar{\gamma}_2$ and $T_2 > T_1$. Then, the line density $(1/\delta_e)$ will be larger in region 2 than in region 1, and $\beta_2 > \beta_1$. The path variations of $\beta(s)$ and $\beta_e(s)$ will be given in Eqs. (48) and (49), but with γ's replaced by β's. Again, in the LS approximation, the emission from ds is assumed to be described by the line density parameter $\beta(s)$ and the attenuation by a homogeneous path with line density parameter $\beta_e(s)$. Clearly, $\beta_e(s) < \beta(s)$ for $s > s_0$. In this case, the radiation from complete lines (rather than from just line wings) will be improperly attenuated in the total

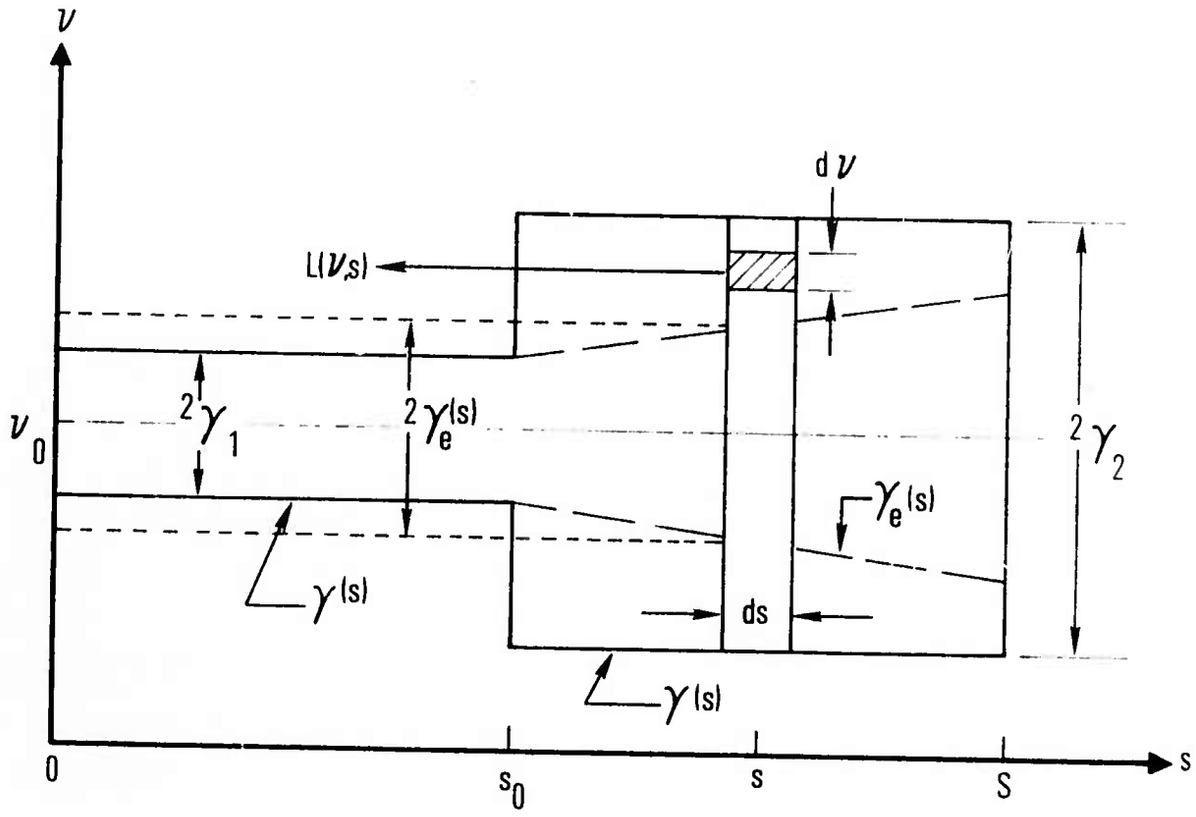

Figure 7. Representation of Two Homogeneous and Isothermal Optical Paths in Series for a Rectangular Line Shape

path radiance computation because each line in region 2 will not have a corresponding line in the attenuation path to s = 0 that can absorb its emission radiation. For region 2 alone, $\beta_e(s) = \beta_2$, and each emission line does have a corresponding absorption line.

The limitation of the LS approximation is that, for optical paths along which $\gamma(s)$ or $\beta(s)$ increases sharply at some point (s_0), the path-averaged quantities $\gamma_e(s)$ or $\beta_e(s)$ do not respond to the change fast enough to give values sufficiently large to properly account for the attenuation of radiation from path elements beyond the region of sharp increase. The solution to this limitation is to allow the attenuation of radiation from ds for $s > s_0$ to be effected by two homogeneous paths that lie between s = 0 and s. The first path is the whole of region 1 ($s = 0$ to $s = s_0$), and the absorption line width or density parameter is taken as the average value for this whole region. The second path is the portion of region 2 between $s = s_0$ and s, and the line width or density parameter is the average value between s_0 and s. The effect is that $\gamma_e(s)$ or $\beta_e(s)$ is able to follow the variations of $\gamma(s)$ or $\beta(s)$ at $s = s_0$ because their computation is begun anew at $s = s_0$ and is not influenced by the properties of the path for $s < s_0$. The formulation of this approach for the Lorentz and Doppler line shape is given in the following sections.

Because the formulations involve two homogeneous paths and derive expressions for the derivative of the equivalent width, the approximation is referred to here as the two-path derivative approximation. The LS approximation corresponds to a single-path derivative approximation. Similarly, the present use of the CG approximation could be considered as a single-path equivalent width approximation. The corresponding two-path equivalent width approximation would be the models presented by Plass.[13, 14]

---

[13] G. N. Plass, "Spectral Band Absorptance of Radiation Traversing Two or More Cells in Series," Appl. Opt. 4, 69 (1965).

[14] G. N. Plass, "The Theory of the Absorption of Flame Radiation by Molecular Bands," Appl. Opt. 4, 161 (1965).

B. FORMULATION FOR LORENTZ LINE SHAPE

The equivalent width derivative for an isolated Lorentz line is

$$\frac{dW(s)}{ds} = c(s)p(s) \int_{-\infty}^{\infty} k(\nu, s) \exp\left[- \int_0^s c(s')p(s')k(\nu, s')\, ds' \right] d\nu \qquad (50)$$

where the spectral absorption coefficient is

$$k(\nu, s) = \frac{S(s)}{\pi} \frac{\gamma(s)}{(\nu - \nu_0)^2 + \gamma^2(s)} \qquad (51)$$

The exponential factor of Eq. (50) describes the attenuation of radiation from the path element ds by the path between s = 0 and s, and it is in the path integral of this factor that the two-path approximation is made. For $s > s_0$, the path integral can be written [by using Eq. (51)] as

$$\int_0^s c(s')p(s')k(\nu, s')\, ds' = \frac{1}{\pi} \int_0^{s_0} \frac{c(s')p(s')S(s')\gamma(s')}{(\nu - \nu_0)^2 + \gamma^2(s')}\, ds'$$

$$+ \frac{1}{\pi} \int_{s_0}^s \frac{c(s')p(s')S(s')\gamma(s')}{(\nu - \nu_0)^2 + \gamma^2(s')} \qquad (52)$$

For the integral between s = 0 and $s = s_0$, $\gamma(s')$ in the denominator of the integrand is replaced by the path-averaged value between s = 0 and $s = s_0$, $\gamma_1(s_0)$. Similarly, for the second integral, $\gamma(s')$ is replaced by the average between $s = s_0$ and s, $\gamma_2(s)$. Then,

$$\int_0^s c(s')p(s')k(\nu,\ s')\,ds' = \frac{2x_1(s_0)}{1 + (\nu - \nu_0)^2/\gamma_1^2(s_0)} + \frac{2x_2(s)}{1 + (\nu_0 - \nu)^2/\gamma_2^2(s)} \tag{53}$$

where

$$x_1(s_0) = \frac{S_1(s_0)\,u_1(s_0)}{2\pi\,\gamma_1(s_0)} \tag{54}$$

$$u_1(s_0) = \int_0^{s_0} c(s')\,p(s')\,ds' \tag{55}$$

$$S_1(s_0) = \frac{1}{u_1(s_0)} \int_0^{s_0} c(s')\,p(s')\,S(s')\,ds' \tag{56}$$

$$\gamma_1(s_0) = \frac{1}{u_1(s_0)\,S_1(s_0)} \int_0^{s_0} c(s')\,p(s')\,S(s')\,\gamma(s')\,ds' \tag{57}$$

$$x_2(s) = \frac{S_2(s)\,u_2(s)}{2\pi\,\gamma_2(s)} \tag{58}$$

$$u_2(s) = \int_{s_0}^{s} c(s')\,p(s')\,ds' \tag{59}$$

$$S_2(s) = \frac{1}{u_2(s)} \int_{s_0}^{s} c(s')\, p(s')\, S(s')\, ds' \tag{60}$$

and

$$\gamma_2(s) = \frac{1}{u_2(s)\, S_2(s)} \int_{s_0}^{s} c(s')\, p(s')\, S(s')\, \gamma(s')\, ds' \tag{61}$$

Substitution of Eq. (53) into (50), the change of variable $z = (\nu - \nu_0)/\gamma(s)$, and the use of the definitions

$$\rho_1(s) = \frac{\gamma(s)}{\gamma_1(s_0)} \tag{62}$$

and

$$\rho_2(s) = \frac{\gamma(s)}{\gamma_2(s)} \tag{63}$$

yield

$$\frac{dW(s)}{ds} = c(s)\, p(s)\, S(s)\, y[\, x_1(s_0),\, x_2(s),\, \rho_1(s),\, \rho_2(s)] \tag{64}$$

where the equivalent width derivative function $y(x_1, x_2, \rho_1, \rho_2)$ is

$$y(x_1, x_2, \rho_1, \rho_2) = \frac{2}{\pi} \int_0^{\infty} \frac{1}{(1 + z^2)} \exp\left[- \frac{2x_1}{1 + z^2 \rho_1^2} - \frac{2x_2}{1 + z^2 \rho_2^2} \right] dz \tag{65}$$

As in the LS approximation, a closed-form solution for Eq. (65) could not be found. However, for bands of lines in which the line strengths are distributed according to an exponential or exponential-tailed inverse line strength distribution, closed-form solutions can be obtained by integrating in the complex z plane by using the method of residues. Arguments presented earlier[3,4] allow the mean equivalent width derivative for bands of lines to be derived as

$$\frac{1}{\delta}\frac{d\overline{W}(s)}{ds} = c(s)\, p(s)\, \overline{k}(s)\, y[x_1(s_0),\ x_2(s),\ \rho_1(s),\ \rho_2(s)] \tag{66}$$

where

$$y[x_1,\ x_2,\ \rho_1,\ \rho_2] = \frac{2}{\pi}\int_0^\infty \frac{dz}{(1+z^2)\left[1+\dfrac{2x_1}{1+z^2\rho_1^2}+\dfrac{2x_2}{1+z^2\rho_2^2}\right]^n} \tag{67}$$

and where $n = 2$ for the exponential line strength distribution and $n = 1$ for the exponential-tailed inverse distribution. The factors that account for compatability with the band model parameter δ_c are suppressed in Eq. (67), but must be included in the final solutions for y. For $n = 2$, both x_1 and x_2 on the right-hand side of Eq. (67) must be multiplied by $\pi/4$; for $n = 1$, they must be multiplied by π. For bands of lines, the x and ρ parameters of Eq. (66) are defined by

$$x_1(s_0) = \frac{\overline{k}_1(s_0)\, u_1(s_0)}{\beta_1(s_0)} \tag{68}$$

$$u_1(s_0) = \int_0^{s_0} c(s')\, p(s')\, ds' \tag{69}$$

$$\bar{k}_1(s_0) = \frac{1}{u_1(s_0)} \int_0^{s_0} c(s')\, p(s')\, \bar{k}(s')\, ds' \tag{70}$$

$$\beta_1(s_0) = \frac{1}{u_1(s_0)\, \bar{k}_1(s_0)} \int_0^{s_0} c(s')\, p(s')\, \bar{k}(s')\, \beta(s')\, ds' \tag{71}$$

$$x_2(s) = \frac{\bar{k}_2(s)\, u_2(s)}{\beta_2(s)} \tag{72}$$

$$u_2(s) = \int_{s_0}^{s} c(s')\, p(s')\, ds \tag{73}$$

$$\bar{k}_2(s) = \frac{1}{u_2(s)} \int_{s_0}^{s} c(s')\, p(s')\, \bar{k}(s')\, ds' \tag{74}$$

$$\beta_2(s) = \frac{1}{u_2(s)\, \bar{k}_2(s)} \int_{s_0}^{s} c(s')\, p(s')\, \bar{k}(s')\, \beta(s')\, ds' \tag{75}$$

$$\rho_1(s) = \beta(s)/\beta_1(s_0) \tag{76}$$

and

$$\rho_2(s) = \beta(s)/\beta_2(s) \tag{77}$$

A straightforward, but tedious, manipulation of Eq. (67) allows it to be written as

$$y(x_1, x_2 \rho_1, \rho_2) = \frac{1}{\pi \rho_1^2 \rho_2^2} \int_{-\infty}^{\infty} \frac{1}{(z - z_1)(z - z_2)} \cdot \left\{ \frac{(1 + \rho_1^2 z^2)(1 + \rho_2^2 z^2)}{(z - z_3)(z - z_4)(z - z_5)(z - z_6)} \right\}^n dz \tag{78}$$

where

$$z_1 = i, \qquad z_2 = -i, \qquad z_3 = \sqrt{p_1},$$

$$z_4 = -\sqrt{p_1}, \qquad z_5 = \sqrt{p_2}, \qquad z_6 = -\sqrt{p_2} \tag{79}$$

$$p_1 = -\frac{b}{2} + \frac{1}{2}\sqrt{b^2 - 4c} \tag{80}$$

$$p_2 = -\frac{b}{2} - \frac{1}{2}\sqrt{b^2 - 4c} \tag{81}$$

$$b = 1 + \frac{2x_1}{\rho_1^2} + \frac{2x_2}{\rho_2^2} \tag{82}$$

and

$$c = \frac{1 + 2(x_1 + x_2)}{\rho_1^2 \rho_2^2} \tag{83}$$

The integration of Eq. (78) by the method of residues is accomplished by closing the contour from $-\infty$ to ∞ by an infinite semicircle in the upper half of the complex z plane. Examination of the integrand of Eq. (78) reveals that the only poles enclosed by the contour are those at z_1, z_3, and z_5. The pole at z_1 is first order, whereas those at z_3 and z_5 are first order for n = 1 and second order for n = 2. The calculation of the residues at z_1, z_2, and z_3 by

$$a_{-1}^{(j)} = \frac{1}{(m-1)!}\left[\frac{d^{m-1}}{dz^{m-1}}\left[(z - z_j)^m I(z)\right]\right]_{z=z_j} \tag{84}$$

where I(z) denotes the integrand of Eq. (78), and m is the order of the pole at z_j, is, again, straightforward but tedious, and only the final result is given. For n = 1 or 2

$$a_{-1}^{(1)} = \frac{(1-\rho_1^2)^n (1-\rho_2^2)^n}{2i\,(1+p_1)(1+p_2)} \tag{85}$$

For n = 1

$$a_{-1}^{(3)} = \frac{(1+\rho_1^2 p_1)(1+\rho_2^2 p_1)}{2i\,(1+p_1)\sqrt{-p_1}\,(p_1-p_2)} \tag{86}$$

and $a_{-1}^{(5)}$ is of the same form, but with p_1 and p_2 interchanged. For n = 2

$$a_{-1}^{(3)} = \frac{1}{2i} \frac{(1 + \rho_1^2 p_1)(1 + \rho_2^2 p_1)}{(1 + p_1)\sqrt{-p_1}(p_1 - p_2)^2}$$

$$\left[2(\rho_1^2 + \rho_2^2) + 4\rho_1^2 \rho_2^2 p_1 - (1 + \rho_1^2 p_1)(1 + \rho_2^2 p_1) \right.$$

$$\left. \times \left(\frac{7p_1^2 - 3p_1 p_2 + 5p_1 - p_2}{2p_1(p_1 - p_2)(1 + p_1)} \right) \right] \qquad (87)$$

and $a_{-1}^{(5)}$ is obtained by interchanging p_1 and p_2. The final formal solution for $y(x_1, x_2, \rho_1, \rho_2)$ is, then

$$y(x_1, x_2, \rho_1, \rho_2) = \frac{2\pi i}{\pi \rho_1^2 \rho_2^2} \left[a_{-1}^{(1)} + a_{-1}^{(3)} + a_{-1}^{(5)} \right] \qquad (88)$$

the 2i factor of Eq. (88) cancels with the 2i factors in the denominators of the a_{-1} terms. It can be verified that, for $x_1 = 0$, $n = 1$, and $x_2 = \pi x$, this solution reduces to the LS approximation solution of Eq. (13).

C. FORMULATION FOR DOPPLER LINE SHAPE

The derivation of the $y(x_1, x_2, \rho_1, \rho_2)$ functions for a Doppler line or bands of Doppler lines follows that for the Lorentz line, except that the Doppler line shape

$$k(\nu, s) = \sqrt{\frac{\ln 2}{\pi}} \frac{S(s)}{\gamma(s)} e^{-\ln 2(\nu - \nu_0)^2 / \gamma^2(s)} \qquad (89)$$

is used. The formal solution for an isolated line is

$$y(x_1, x_2, \rho_1, \rho_2) = \frac{2}{\pi}\int_0^\infty \exp\left[-z^2 - x_1 e^{-\rho_1^2 z^2} - x_2 e^{-\rho_2^2 z^2}\right] dz \qquad (90)$$

For the exponential (n = 2) and exponential-tailed inverse (n = 1) line strength distributions

$$y(x_1, x_2, \rho_1, \rho_2) = \frac{2}{\sqrt{\pi}}\int_0^\infty \frac{e^{-z^2}}{\left[1 + x_1 e^{-\rho_1^2 z^2} + x_2 e^{-\rho_2^2 z^2}\right]^n} \qquad (91)$$

The definitions for the path averages are the same as for the Lorentz case, Eqs. (54) through (63) and (68) through (77), except that x_1 and x_2 are given by equations of the form

$$x = \sqrt{\frac{\ln 2}{\pi}}\,\frac{Su}{\gamma}$$

for the insolated line case, Eqs. (54) and (58), respectively. The factors $\pi/4$ for n = 2 and π for n = 1 have been suppressed in Eq. (91).

Neither Eq. (90) nor (91) is amenable to closed-form solutions. In the LS approximation, tables of values were prepared from which the desired value could be interpolated. However, even this method is not practical here because there are now four independent variables (x_1, x_2, ρ_1, and ρ_2) rather than just the two (x, ρ) of the LS approximation on which to interpolate. Tables for adequate ranges of the four variables would be prohibitively voluminous. The solution used here is to approximate the Doppler line shape by a parabolic line shape. This approximation is applied and discussed in the following section.

D. FORMULATION FOR PARABOLIC LINE SHAPE

The spectral absorption coefficient for a parabolic line shape is

$$k(\nu, s) = \begin{cases} \frac{3}{4\sqrt{2}} \frac{S(s)}{\gamma(s)} \left[1 - \frac{(\nu - \nu_0)^2}{2\gamma^2(s)} \right] & | \nu - \nu_0 | \leq \sqrt{2}\, \gamma(s) \\ 0 & | \nu - \nu_0 | > \sqrt{2}\, \gamma(s) \end{cases} \tag{92}$$

In order to approximate the Doppler line shape by the parabolic line shape, the line strength S(s) and the value of $k(\nu, s)$ at the line center are chosen to be the same for the two profiles. This requires that the parabolic line width be chosen as

$$\gamma_P = \frac{3}{4\sqrt{2}} \sqrt{\frac{\pi}{\ln 2}}\, \gamma_D = 1.127\, \gamma_D \tag{93}$$

where γ_D is the Doppler line width. The resulting profile approximation is shown in Fig. 8

The rationale for using the parabolic approximation is threefold. First, for many applications, account of Doppler broadening provides only a small correction to the radiative transfer effects computed with the Lorentz line shape. The error inherent in using a parabolic rather than Doppler profile to compute this small correction term is thus minimized. Second, for many cases where the Doppler effect is the dominant line-broadening mechanism, the absorption for the path is small. For weak absorption, radiative transfer effects are independent of line shape and depend only on the line strength. Third, closed-form solutions can be obtained for the parabolic line shape.

Following the procedure for the Lorentz line, the equivalent width derivative function for an isolated parabolic line is

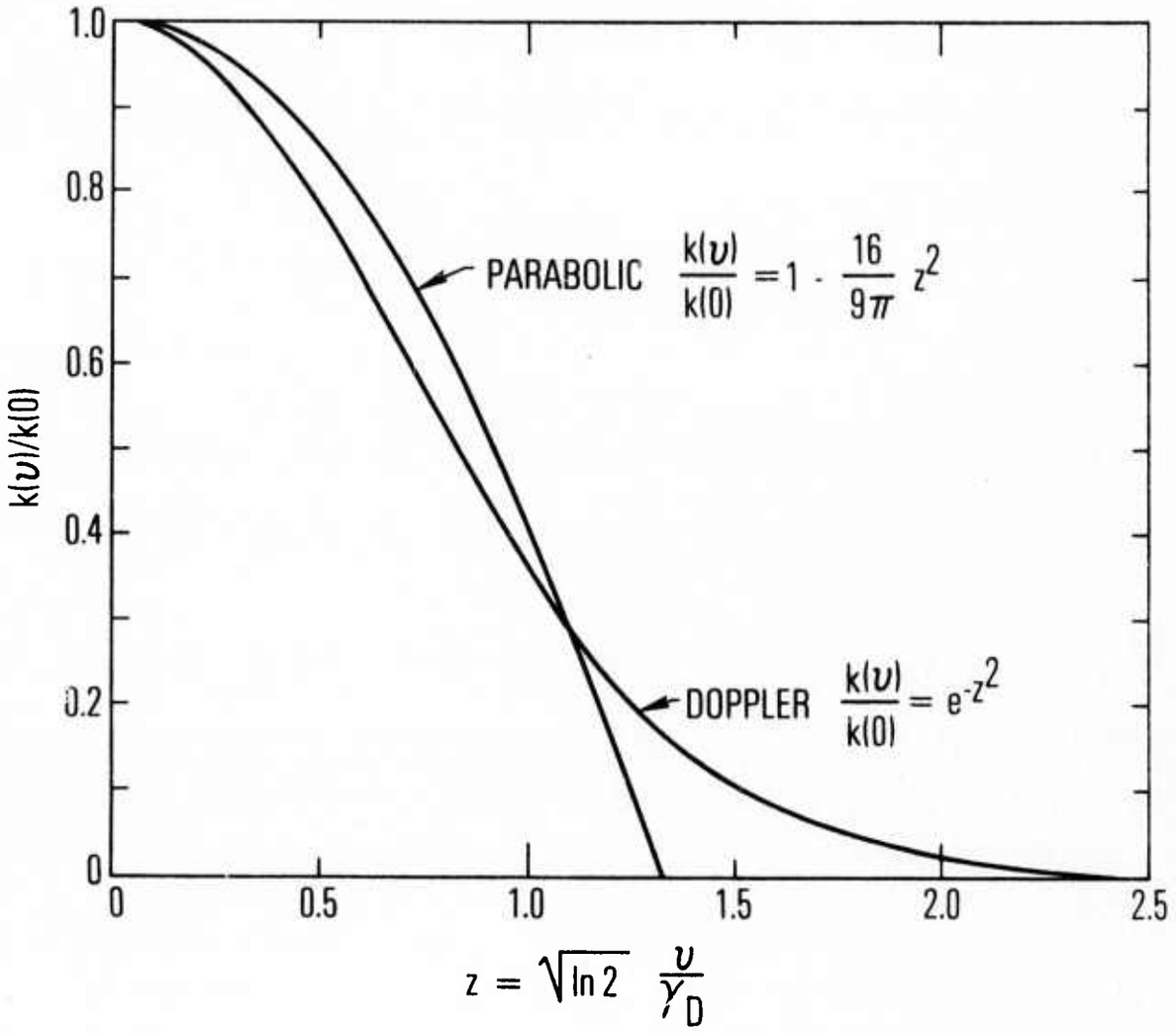

Figure 8. Comparison of Doppler and Parabolic Line Profiles for Forced Correspondence of Line Strength and Line Center Absorptance

$$y(x_1, x_2, \rho_1, \rho_2) = \frac{3}{2}\int_0^\infty (1 - z^2) \exp\left[- x_1(1 - \rho_1^2 z^2) - x_2(1 - \rho_2^2 z^2)\right] dz \qquad (94)$$

For bands of lines

$$y(x_1, x_2, \rho_1, \rho_2) = \frac{3}{2}\int_0^\infty \frac{(1 - z^2)}{\left[1 + x_1(1 - \rho_1^2 z^2) + x_2(1 - \rho_2^2 z^2)\right]^n} dz \qquad (95)$$

Again, the parameters x_1, x_2, ρ_1, and ρ_2 are defined by equations of the form given for the Lorentz line case, but with x_1 and x_2 defined by the form

$$x = \frac{3}{4\sqrt{2}} \frac{Su}{\gamma}$$

for isolated lines. In all cases, γ is the parabolic line width. Again, the $\pi/4$ and π factors for $n = 2$ and 1, respectively, are suppressed in Eq. (95).

The infinite integration limits of Eqs. (94) and (95) are formal limits only. Because the parabolic line shape has a discontinuous slope at the point where it goes to zero, the integration of Eqs. (94) or (95) must be handled as a set of six cases, which result from the six inequality relations that can be formed among the three line widths $\gamma_1(s_0)$, $\gamma_2(s)$, and $\gamma(s)$. Other than the tedium of keeping track of these cases, the integrations are all elementary, and the result for all cases can be written as

$$y(x_1, x_2, \rho_1, \rho_2) =$$

$$= \begin{cases} g(x_1, x_2, \rho_1, \rho_2, 0, 1) & \rho_2 \le \rho_1 \le 1 \\ g(x_1, x_2, \rho_1, \rho_2, 0, 1/\rho_1) + g(0, x_2, \rho_1, \rho_2, 1/\rho_1, 1) & \rho_2 \le 1 \le \rho_1 \\ g(x_1, x_2, \rho_1, \rho_2, 0, 1/\rho_1) + g(0, x_2, \rho_1, \rho_2, 1/\rho_1, 1/\rho_2) + g_0(\rho_2) & 1 \le \rho_2 \le \rho_1 \\ g(x_1, x_2, \rho_1, \rho_2, 0, 1) & \rho_1 \le \rho_2 \le 1 \\ g(x_1, x_2, \rho_1, \rho_2, 0, 1/\rho_2) + g(x_1, 0, \rho_1, \rho_2, 1/\rho_2, 1) & \rho_1 \le 1 \le \rho_2 \\ g(x_1, x_2, \rho_1, \rho_2, 0, 1/\rho_2) + g(x_1, 0, \rho_1, \rho_2, 1/\rho_2, 1/\rho_1) + g_0(\rho_1) & 1 \le \rho_1 \le \rho_2 \end{cases} \tag{96}$$

For an isolated line, or band of equal intensity lines

$$g(x_1, x_2, \rho_1, \rho_2, a, b) = \frac{3e}{4x}^{-(x_1+x_2)} \left[a \left\{ 1 - \frac{(1 + 2x)\, D(a\sqrt{x})}{a\sqrt{x}} \right\} e^{a^2 x} - b \left\{ 1 - \frac{(1 + 2x)\, D(b\sqrt{x})}{b\sqrt{x}} \right\} e^{b^2 x} \right] \tag{97}$$

and

$$g_0(\rho) = (\rho - 1)^2 (2\rho + 1)/2\rho^3 \tag{98}$$

where $x = x_1\rho_1^2 + x_2\rho_2^2$, and $D(\eta)$ is Dawson's function

$$D(\eta) = e^{-\eta^2} \int_0^{\eta} e^{u^2}\, du \tag{99}$$

For a band of parabolic lines with an exponential line strength distribution (n = 2)

$$g(x_1, x_2, \rho_1, \rho_2, a, b) = \frac{3}{2}\frac{x - \alpha}{2\alpha x}\left[\frac{(b - a)(\alpha + abx)}{(\alpha - a^2 x)(\alpha - b^2 x)} + \frac{1}{\sqrt{\alpha x}} \ln \left\{\frac{\alpha + b\sqrt{\alpha x}}{\alpha - b\sqrt{\alpha x}} \quad \frac{\alpha - a\sqrt{\alpha x}}{\alpha + a\sqrt{\alpha x}}\right\}\right] \tag{100}$$

and

$$g_0(\rho) = \frac{\rho - 1}{2\rho^3}(\rho^2 - 2\rho - 2) \tag{101}$$

where $\alpha = 1 + x_1 + x_2$.

For the exponential-tailed inverse distribution

$$g(x_1, x_2, \rho_1, \rho_2, a, b) = \frac{3}{2}\left[\frac{b - a}{x} + \frac{(x - \alpha)}{2x\sqrt{\alpha x}} \ln \left\{\frac{\alpha + b\sqrt{\alpha x}}{\alpha - b\sqrt{\alpha x}} \quad \frac{\alpha - a\sqrt{\alpha x}}{\alpha + a\sqrt{\alpha x}}\right\}\right] \tag{102}$$

and

$$g_0(\rho) = \frac{\rho - 1}{2\rho^3}(\rho^2 - 2\rho - 2) \tag{103}$$

E. RESULTS AND DISCUSSION

The calculations with the two-path derivative approximation were performed exactly as for the CG and LS approximations, except that for $s > s_0$, y was computed according to Eq. (88) rather than Eqs. (11) or (13) for the Lorentz component of the line and to Eqs. (96) and (102) rather than Eq. (16) or Table 1 for the Doppler (parabolic) component. Also, for $s > s_0$, the weak-limit form of the equivalent width, required in the combining of the Lorentz and Doppler (parabolic) components to give the Voigt line result, was taken as

$$\frac{\overline{W}_W(s)}{\delta} = u_1(s_0)\,\overline{k}_1(s_0) + u_2(s)\,\overline{k}_2(s) \tag{104}$$

The variation of T_e with altitude for the three bandpasses is shown in Fig. 9. The results for the Lorentz line component are indistinguishable from those obtained with the LS approximation. The largest difference that occurred between T_e computed with the two approximations was ~ 4 percent. The results for the Doppler line component show a substantial improvement over those obtained with either the CG or LS approximations. The variation with altitude is physically realistic for the whole altitude region. Spectra $\overline{\tau}_e(\nu)$ for the Doppler line shape and z = 30 km are shown in Fig. 10 for all three inhomogeneity approximations.

For all three bandpasses, the result for the Voigt line shape displays a smooth transition from the Lorentz curve at $z \simeq 15$ km to the Doppler curve at $z \simeq 50$ km, although only for the low wavenumber bandpass is the transition to the Doppler curve complete. As for the LS approximation, the Voigt result always lies between the Lorentz and Doppler results.

Spectra of $\overline{\tau}_e(\nu)$ computed for each line shape and for z = 35 km are presented in Fig. 11. To within calculational accuracy, the Voigt line shape spectrum always lies between the spectra for the Lorentz and Doppler line components or, in the band wing regions, is the same as the Doppler spectrum.

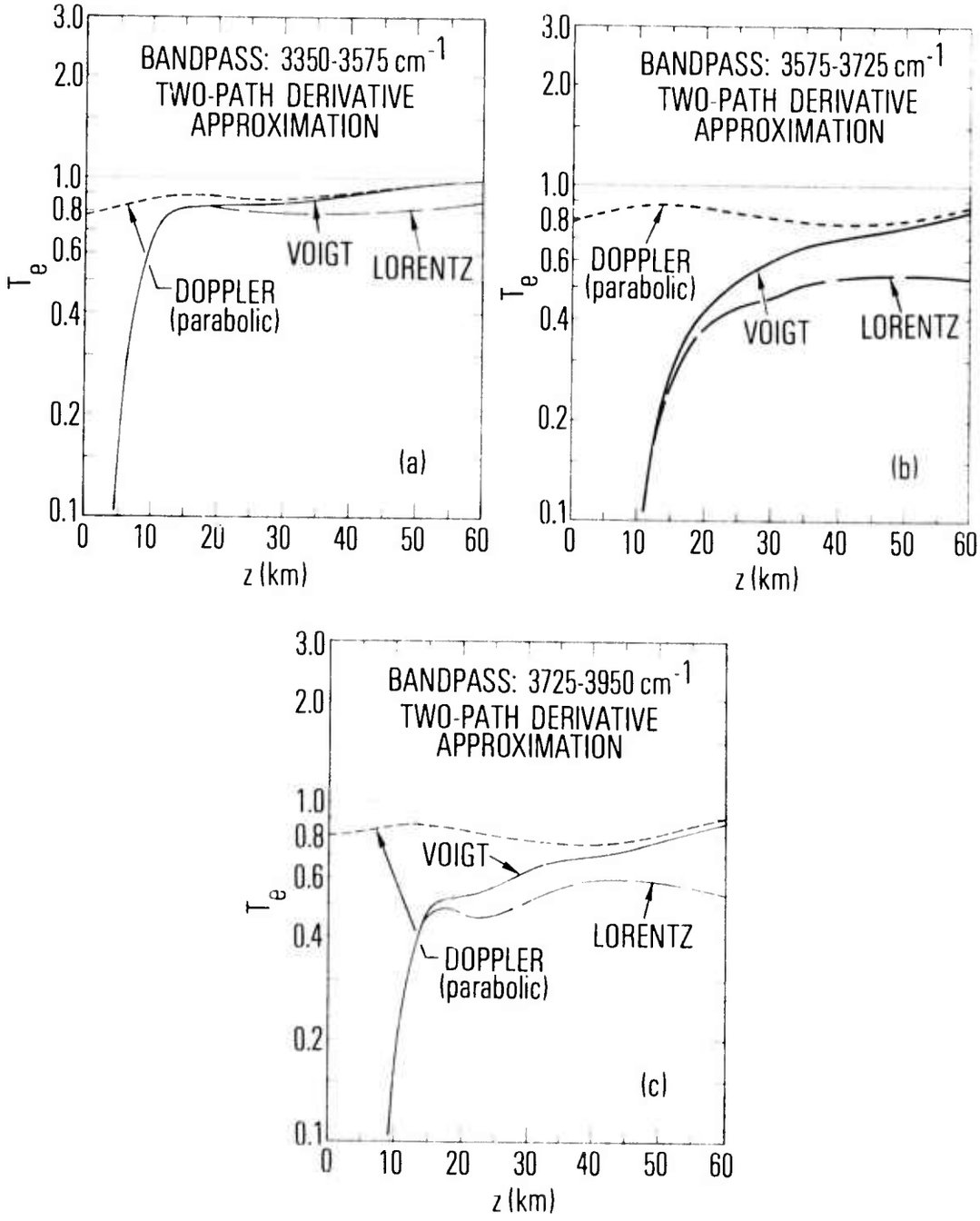

Figure 9. Altitude Variation of T_e Computed for the Lorentz, Doppler, and Voigt Line Shapes and with the Two-Path Derivative Approximation. (a) 3350-3575 cm^{-1} bandpass; (b) 3575-3725 cm^{-1} bandpass; (c) 3725-3950 cm^{-1} bandpass.

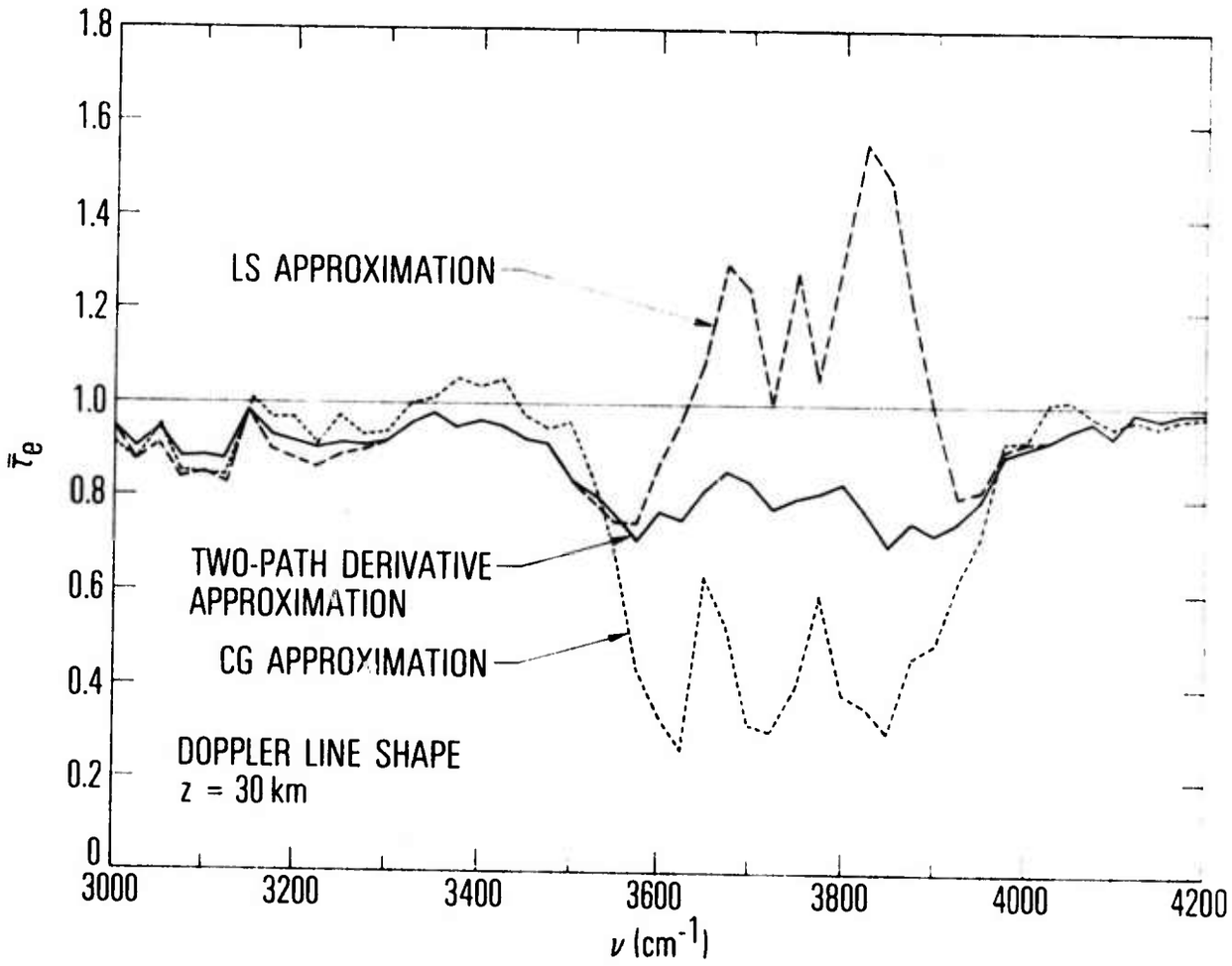

Figure 10. Spectral Variation of $\bar{\tau}(\nu)$ at z = 30 km Computed for the Doppler Line Shape and with the CG, LS, and Two-Path Derivative Approximations. For the latter approximation, the line shape is assumed to be parabolic.

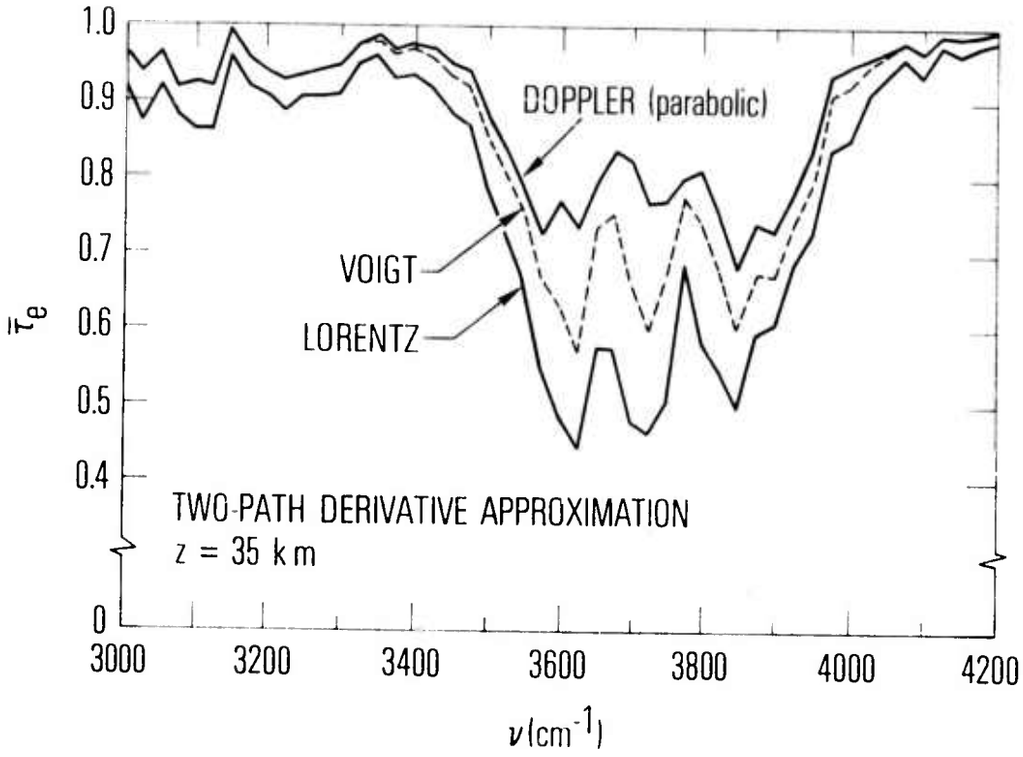

Figure 11. Spectral Variation of $\bar{\tau}_e(\nu)$ at z = 35 km Computed for the Lorentz, Doppler, and Voigt Line Shapes and with the Two-Path Derivative Approximation

The two-path derivative approximation provides a significant improvement over the LS approximation for the Doppler line shape, but not for the Lorentz line shape, at least for the problem considered here. This effect is most probably a result of the relative shapes of the two line profiles. The Doppler line has little wing structure and more closely resembles a rectangular line (for which the LS approximation is worst) than does the Lorentz line shape.

In Fig. 12, the 3575-3725 cm^{-1} bandpass result for T_e computed for the Voigt line shape with the two-path derivative approximation is shown together with the atmospheric transmittance T for the same line shape and bandpass. The transmittance T is the correct transmittance to use for computation of the attenuation that continuum radiation (such as black body radiation) or line emission from any molecular species other than CO_2 or H_2O would experience in traversing the atmospheric path from the altitude z to space. For continuum radiation, line correlation is a meaningless concept, whereas for non-H_2O or CO_2 radiation, the line arrangement between the emission spectrum and the absorption spectrum is almost certain to be uncorrelated. This transmittance approaches unity rapidly and is greater than 0.95 for all $z \geq 40$ km. For all continuum radiation sources (or non-H_2O/CO_2 gaseous emitters) above $\sim$ 40 km, the atmosphere can thus be considered as transparent. For the hot H_2O/CO_2 plume model source used here, the correct attenuation factor is T_e. Its value of $\sim$ 0.7 at 40 km can hardly be considered as representative of a transparent atmosphere. Even at the maximum altitude considered here (z = 60 km), T_e has obtained a value of only $\sim$ 0.83. At 60 km, on the other hand, T is nearly 0.99. Now that Doppler broadening effects have been realistically accounted for by using the two-path derivative approximation, this remaining large difference between T and T_e can be attributed only to line correlation effects that exist between the hot H_2O/CO_2 emission spectrum and the cool H_2O/CO_2 atmospheric absorption spectrum.

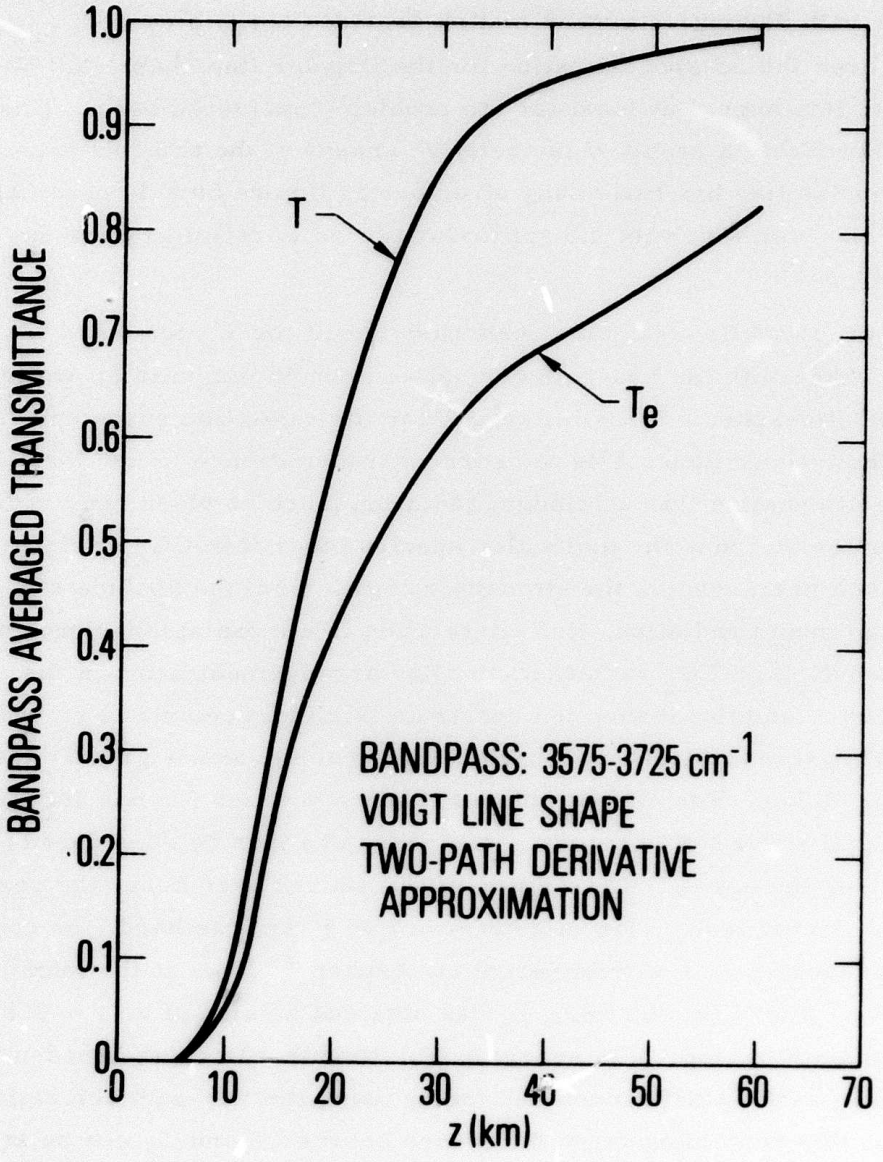

Figure 12. Altitude Variation of T and T_e for the 3575-3725 cm^{-1} Bandpass Computed for the Voigt Line Shape and with the Two-Path Derivative Approximation

LABORATORY OPERATIONS

The Laboratory Operations of The Aerospace Corporation is conducting experimental and theoretical investigations necessary for the evaluation and application of scientific advances to new military concepts and systems. Versatility and flexibility have been developed to a high degree by the laboratory personnel in dealing with the many problems encountered in the nation's rapidly developing space and missile systems. Expertise in the latest scientific developments is vital to the accomplishment of tasks related to these problems. The laboratories that contribute to this research are:

Aerophysics Laboratory: Launch and reentry aerodynamics, heat transfer, reentry physics, chemical kinetics, structural mechanics, flight dynamics, atmospheric pollution, and high-power gas lasers.

Chemistry and Physics Laboratory: Atmospheric reactions and atmospheric optics, chemical reactions in polluted atmospheres, chemical reactions of excited species in rocket plumes, chemical thermodynamics, plasma and laser-induced reactions, laser chemistry, propulsion chemistry, space vacuum and radiation effects on materials, lubrication and surface phenomena, photosensitive materials and sensors, high precision laser ranging, and the application of physics and chemistry to problems of law enforcement and biomedicine.

Electronics Research Laboratory: Electromagnetic theory, devices, and propagation phenomena, including plasma electromagnetics; quantum electronics, lasers, and electro-optics; communication sciences, applied electronics, semiconducting, superconducting, and crystal device physics, optical and acoustical imaging; atmospheric pollution; millimeter wave and far-infrared technology.

Materials Sciences Laboratory: Development of new materials; metal matrix composites and new forms of carbon; test and evaluation of graphite and ceramics in reentry; spacecraft materials and electronic components in nuclear weapons environment; application of fracture mechanics to stress corrosion and fatigue-induced fractures in structural metals.

Space Physics Laboratory: Atmospheric and ionospheric physics, radiation from the atmosphere, density and composition of the atmosphere, aurorae and airglow; magnetospheric physics, cosmic rays, generation and propagation of plasma waves in the magnetosphere; solar physics, studies of solar magnetic fields; space astronomy, x-ray astronomy; the effects of nuclear explosions, magnetic storms, and solar activity on the earth's atmosphere, ionosphere, and magnetosphere; the effects of optical, electromagnetic, and particulate radiations in space on space systems.

THE AEROSPACE CORPORATION
El Segundo, California